ANL-6789
Reactor Technology
(TID-4500, 30th Ed.)
AEC Research and
Development Report

ARGONNE NATIONAL LABORATORY
9700 South Cass Avenue
Argonne, Illinois 60440

THE BREEDING RATIO OF A PLUTONIUM LOADING IN EBR-I

by

R. R. Smith, R. O. Haroldsen,
R. E. Horne,* and R. G. Matlock**

Idaho Division

*Atomic Power Development Associates, Inc., Detroit, Michigan
**University of Colorado, Boulder, Colorado

February 1964

Operated by The University of Chicago
under
Contract W-31-109-eng-38
with the
U. S. Atomic Energy Commission

DISCLAIMER

TABLE OF CONTENTS

TABLE OF CONTENTS

TABLE OF CONTENTS

LIST OF FIGURES

LIST OF FIGURES

LIST OF TABLES

THE BREEDING RATIO OF A PLUTONIUM-LOADING IN EBR-I

by

R. R. Smith, R. O. Haroldsen,
R. E. Horne,*and R. G. Matlock**

I. INTRODUCTION

During the mid- and late 1940's, sufficient information was available to conclude that a reactor could be designed to produce at least as much fuel as it consumed and at the same time generate useful power. The economic advantages of such a system were clear, for implicit in this concept was the promise that huge accumulations of essentially worthless U^{238} could eventually be converted to valuable reactor fuel.

To establish the validity of the breeding principle and to demonstrate the operational feasibility of small, highly concentrated, liquid metal-cooled cores, a first-generation fast reactor, EBR-I, was designed and placed in operation at the National Reactor Testing Station in Idaho.[1-6] As a result of a broad background of operational experience with this facility, considerable progress has been made in solving many problems peculiar to this reactor type.[7-12]

Of particular interest to the designer of such systems is the parameter commonly called the conversion ratio (or breeding ratio), defined loosely as the ratio of fuel returned to the system to the amount destroyed. Levenson,[13] Curtis et al.,[14] and Kato et al.,[15] demonstrated, in their experiments with EBR-I, that conversion ratios greater than unity can be achieved in practice. Since the EBR-I was not specifically designed for high conversion ratios, production of fuel at a rate at least equal to the consumption rate is significant.

In the current (fourth) loading of EBR-I, metallic plutonium stabilized with 1.25 w/o aluminum is used as the fuel material. In the previous three loadings, metallic uranium enriched in the U^{235} isotope was used as fuel. Since the values of ν and α for plutonium are more conducive to breeding, a higher value of the breeding ratio is expected. The measurement of this important parameter for the present plutonium-fueled core is the subject of this report.

II. DESCRIPTION OF MARK-IV LOADING

Since subsequent discussions rely on some knowledge of the physical characteristics of the reactor, it seems advisable to describe briefly those

*APDA, Detroit, Michigan.

**Physics Dept., U. of Colorado, Boulder, Colorado.

features which affect an understanding of the physical relationship of fuel and blanket material. A more detailed description of the reactor and support systems has been given.[16]

A. Mark-IV Fuel Rods

Details pertaining to the Mark-IV fuel rods are shown in Fig. 1. A fuel rod consists essentially of a slug-filled Zircaloy-2 tube having an outside diameter of 0.299 in. and a wall thickness of 0.021 in. Three equally spaced Zircaloy-3 ribs, each 0.049 in. in height, run longitudinally along the active portion of the rod. The ribs serve three purposes: they provide uniform spacing, ensure maximum radial coupling between rods, and prevent rod-deformation effects.

The fuel portion of the rod consists of four plutonium-aluminum alloy slugs, each 2.121 in. long, for a total core height of 8.484 in. Depleted uranium slugs, 7.745 and 3.552 in. in length, located above and below the fuel portion, define the upper and lower axial blankets, respectively. All fuel slugs are 0.232 in. in diameter, whereas blanket slugs are 0.235 in. in diameter. Die-formed spacing ribs on the surface of the fuel slugs position them concentrically in the jackets. A 0.0125-in., NaK-filled annulus between the slugs and jackets serves as a heat-transfer bond.

The fuel consists of an alloy which has the following weight-percent composition: plutonium, 98.59; aluminum, 1.25; and impurities (Fe, Cr, and Cu), 0.16. On an atomic basis, this composition is equivalent to 90.0 a/o plutonium.

The fuel was fabricated from two batches of feed material. One batch, approximately two-thirds of the total, had the following isotopic composition: Pu^{239}, 95.1%; Pu^{240}, 4.5%; Pu^{241}, 0.44%; and Pu^{242}, a trace. The second batch had the following composition: Pu^{239}, 93.2%; Pu^{240}, 6.2%; Pu^{241}, 0.55%; and Pu^{242}, a trace. The average density of the alloy (either batch) was 15.03 ± 0.05 g/cm^3.[17]

B. Mark-IV Blanket Rods

To fill out the provided positions not occupied by fuel in the inner seven hexes, special blanket rods (termed Mark-IV) are needed. With the exception that blanket material is substituted for fuel, these rods are essentially identical with those containing fuel. The active section of the rod consists of four slugs of depleted uranium, all 0.235 in. in diameter: one 7.745 in., two 4.247 in., and one 3.552 in. in length. For all Mark-IV rods, the unit loading per hex is 60 fuel or blanket rods and a centrally located expandable tightening rod.

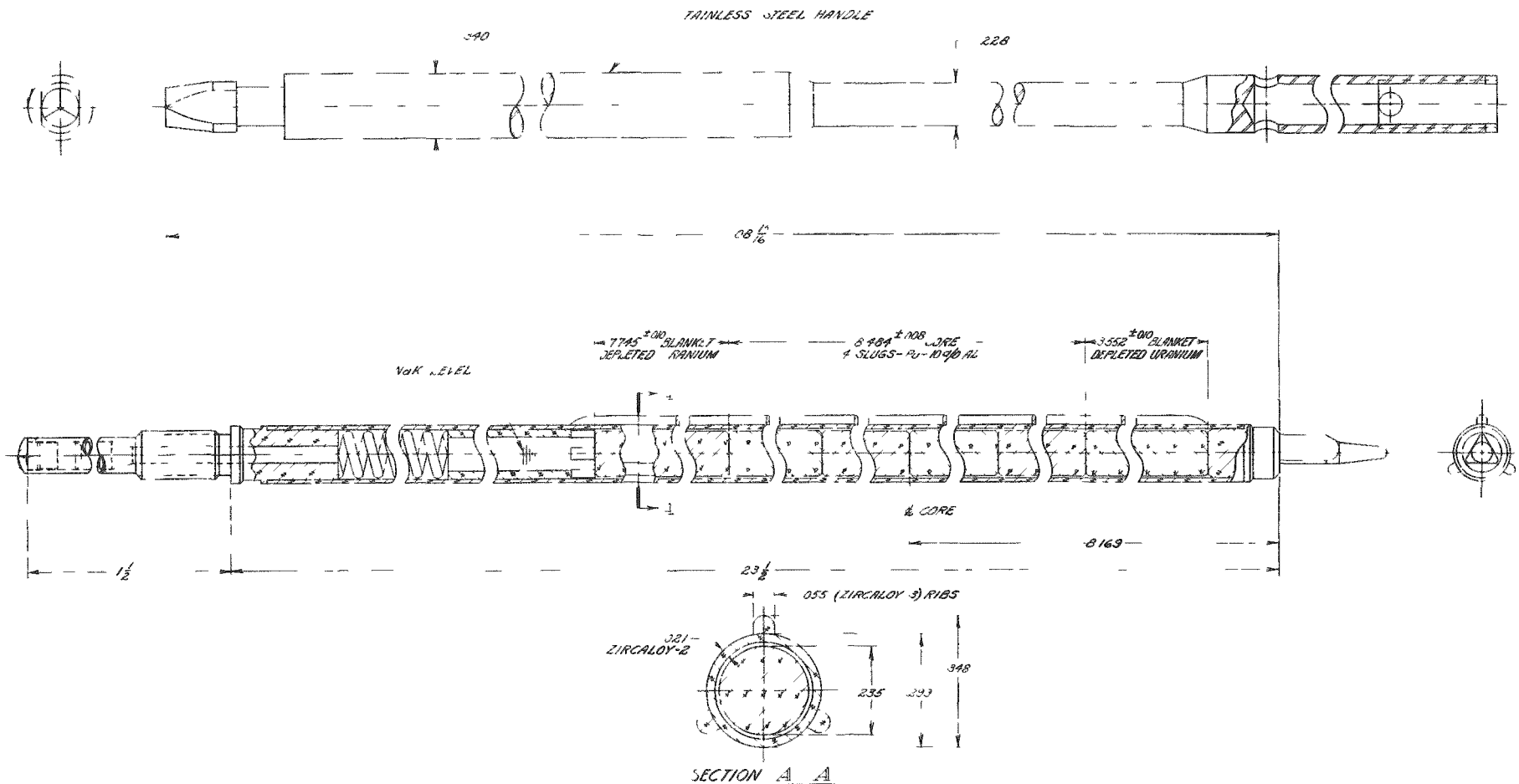

Fig. 1. Mark-IV Fuel Rod

C. Mark-III Blanket Rods

The blanket material, consisting of an alloy of 98 w/o natural uranium and 2 w/o zirconium, has a density of approximately 17.95 g/cm^3. Cladding consists of 0.020 in. of Zircaloy-2, metallurgically bonded to the alloy by a coextrusion process. A typical rod OD is 0.404 in., resulting in an OD of 0.364 in. for the blanket material. The length of the active portion of a blanket rod is $19\frac{13}{16}$ in. For hexes containing Mark-III blanket rods, the unit loading per hex is 36 rods and a centrally located expandable tightening rod.

D. Hexes

A typical fuel or blanket assembly consists of a hexagonally shaped stainless steel tube, 2.875 in. across the flats, with a wall thickness of 0.040 in. Nineteen of these assemblies (a central one, an inner ring of six, and an outer ring of twelve) are arranged hexagonally to define the core and inner radial blanket. Details of the arrangement are shown in Fig. 2, which represents a horizontal cross section through the inner tank assembly. Of 420 positions available in the inner seven assemblies, 320 (all centrally located) are filled with fuel rods. The remaining 100 are filled with Mark-IV blanket rods. The outer ring of 12 hexes is filled completely with Mark-III blanket rods.

E. Reference Loading

The reference loading for the breeding gain measurements is also illustrated in Fig. 2. As discussed in Section A above, the fuel material involves two batches, each different in isotopic content. However, inventory figures, available for each fuel rod, permit the total weight of each major plutonium isotope to be evaluated. Hence, the inventory associated with the 320-fuel-rod reference loading is broken down as follows: total plutonium, 28.100 kg; Pu^{239}, 26.540 kg; Pu^{240}, 1.423 kg; Pu^{241}, 0.137 kg. In the evaluation of the breeding gain, it was assumed that these quantities were uniformly distributed throughout the volume of the core.

F. Outer Radial Blanket

Surrounding the inner tank assembly is the massive outer blanket (or cup) consisting of 84, keystone-shaped natural uranium bricks arranged in 12 stacks of seven (see Fig. 3). To prevent oxidation of the uranium, each brick is clad with 0.020 in. of stainless steel. Each brick is penetrated by five one-in. holes through which cooling air is forced. A single 2-in. hole in each brick serves as a passage for a safety rod or a control rod, made of stainless steel-clad natural uranium metal. The entire assembly is mounted on a pedestal which may be raised or lowered relative to the core. The cup serves as a coarse control of reactivity, as a strong shut-down capability, and as a massive fertile region for generating plutonium.

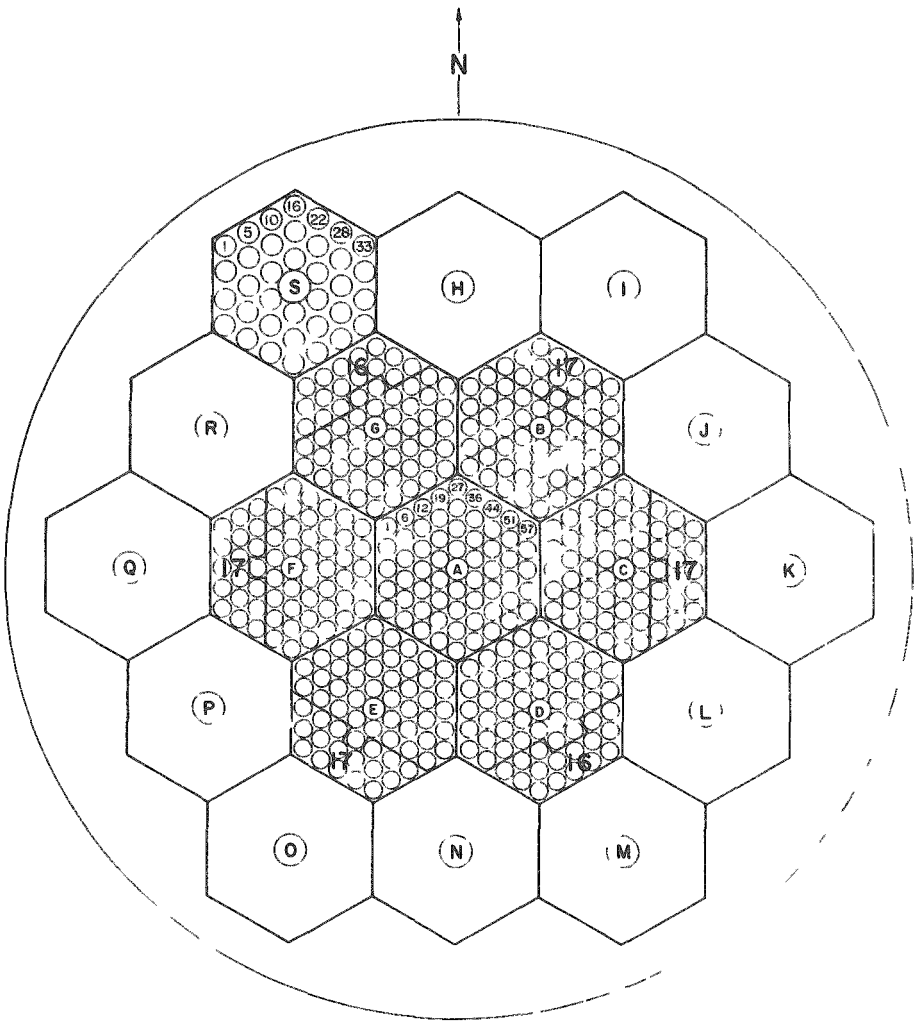

Fig. 2. Horizontal Cross Section through EBR-I, Mark-IV Reference Loading

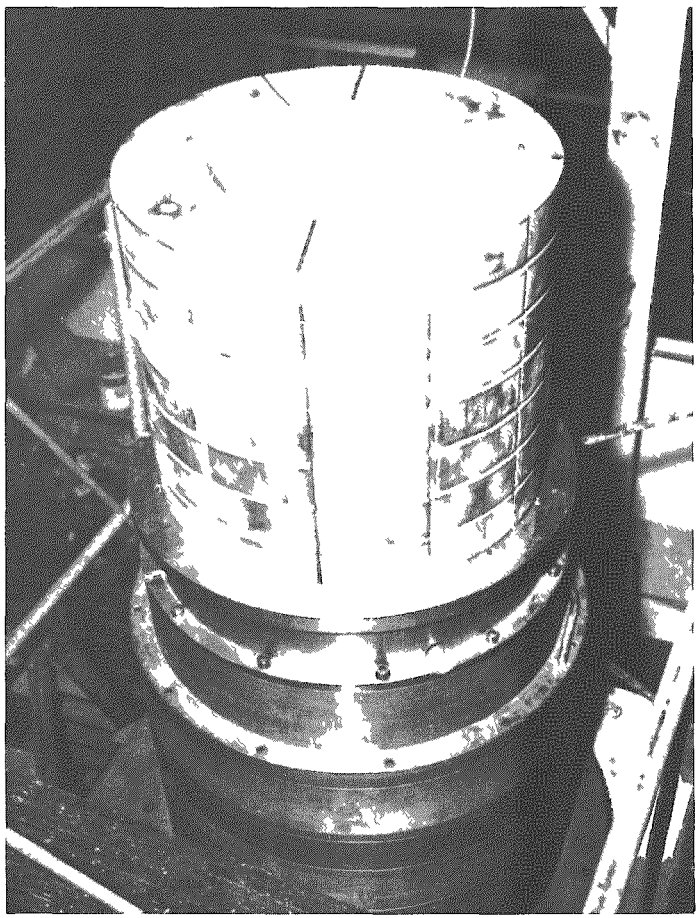

Fig. 3. Outer Blanket

III. DEFINITION OF BREEDING

The distinction between conversion and breeding is clearly drawn. In conversion, the fissionable material generated differs chemically and isotopically from the original fuel. The previous three loadings in EBR-I may be used as illustrations of the conversion process, for in these loadings the end product, Pu^{239}, was produced at the expense of U^{235}. In "breeding," on the other hand, the fissionable product is chemically and isotopically identical with the fuel. According to this definition, the Mark-IV loading in EBR-I is a true breeding system, since the product, Pu^{239}, is identical with the fuel.

Unfortunately, the definitions for conversion and breeding ratios are not so easily established. In fact, popular usage of these terms has been so loose that Spinrad[18] considered it necessary to define these and related terms in considerable detail. According to Spinrad, the commonly defined conversion (or breeding) ratio, which compares the number of fissionable atoms produced to the number of original fissionable atoms destroyed, is actually a misnomer and should more properly be referred to as the "fool's conversion ratio." He objected to this definition because the fissionable material produced is not necessarily the same as the fuel, and the ratio so defined has meaning only for a time close to zero. To avoid ambiguity, he proposed that breeding have a meaning only when the fissionable material produced is the same as the fissionable material destroyed, and that breeding be a process defined only for a fuel cycle at steady-state conditions. He further defined the term "steady state" as a long-time average of all variables pertinent to an evaluation of the breeding ratio. Accordingly, the definition commonly used for conversion ratio (i.e., the fool's conversion ratio) should more properly be identified as the initial conversion ratio.

In discussing definitions, Spinrad pointed out that individuals, depending on their disciplines, may choose other criteria as figures of merit. This would lead logically to such terms as the "freshman chemist's breeding ratio," the "mass spectroscopist's breeding ratio," and the "physicist's breeding ratio." Rather than follow the details of the definitions, which are not simple, the reader is referred to Spinrad's discussion.

The definition used for breeding ratio in this report is given by the following:

$$\text{Breeding ratio} = \frac{\text{Fissionable material produced}}{\text{Fissionable material destroyed}}, \qquad (1)$$

where the numerator consists of the total quantity of fissionable material produced (i.e., Pu^{239} and Pu^{241}) in the system, and the denominator defines

the total amount of fissionable material destroyed (i.e., Pu^{239}, Pu^{241}, and U^{235}). Of necessity, the breeding ratio so defined and evaluated in these measurements should more properly be identified as the initial breeding ratio, since all measurements were carried out under non-steady-state conditions.

Although the purist may object, the defense of this definition rests on the following arguments: (1) previous definitions of conversion in EBR-I were similarly premised; and (2) sufficient experimental information will be given to permit the more conscientious reader to evaluate his own choice of breeding ratio. Inherent in the use of equation (1) as a definition is the philosophy that since the definition is clear and understood, it will serve as a useful criterion of breeding efficiency.

IV. EXPERIMENTAL METHODS

A. Choice of Method

Information necessary for evaluating the breeding ratio may be obtained through either chemical or physical measurements. Each method is based on an integration of various fission and capture patterns over the entire volume of the system. The two methods differ only in the manner used to establish the various profiles. The chemical method, although capable of at least the same accuracy as the physical method, suffers from a serious disadvantage: the reactor must be operated long enough to produce measurable concentrations of plutonium throughout the various blankets. As a result, the generation of substantial quantities of fission products greatly complicates the necessary chemical analyses. For this reason, the chemical method was rejected.

Physical measurements, in contrast, yield essentially the same information from studies carried out at relatively low levels of power. The experimenter may also choose between two reasonably well-established techniques. One is the counter-traverse method, which involves mapping fission patterns throughout the core and blanket regions with small fission counters loaded with appropriate materials. The other technique is based on the observation of activities generated in thin metallic foils of uranium and plutonium. In principle, both methods seem capable of yielding equally reliable information. In practice, the problems associated with the development, fabrication, and perfection of extremely small, yet rugged, fission counters are formidable. For this reason alone, the foil activation method was regarded as the more practical.

B. Equipment

Two major items of counting equipment were used during the measurements. In the earlier, exploratory phases, a 512-channel pulse-height analyzer was used as a qualitative tool for comparing various spectra. In later phases, when the multichannel feature was not needed, all counting operations were carried out with a single-channel analyzer.

1. Multichannel Analyzer

The equipment used was a Model ND-120 512-channel Nuclear Data Analyzer which received pulses from a Type S Harshaw Integral Line scintillator. The latter consisted of a 2 x 2-in. Type S thallium-activated NaI crystal optically coupled to a Dumont 6292 photomultiplier tube. After a 2-week period of high-voltage "seasoning," drifts (directly attributable to aging effects in the detector assembly) were found to be small.

2. Single-channel Analyzer

The equipment used for counting the various foils consisted essentially of a Model SC-77 Tracerlab spectrometer. A Type S Harshaw Integral Line crystal photomultiplier unit, mounted vertically in a cylindrical lead shield, was used as the detector. Rectangular aluminum trays which fitted into a castle-type tray holder were used to position the foils for counting. To ensure uniform placement of the foils, a depression, approximately 0.020 in. deep and 0.220 in. in diameter, was milled at the geometrical center of the tray.

The electronic features of the spectrometer were as follows:

a. Recovery time was less than 7 μsec for an overload 250 times the input.

b. Resolving time for integral operation was approximately 1.2 μsec.

c. Threshold stability was less than 0.5 V for a 10 percent change in line voltage.

d. There was no threshold drift for gross counting rates less than 2×10^5 c/sec.

e. A switching feature permitted both integral and differential counting.

Tests of the upper and lower discriminator levels with a precision pulse generator over several hours did not indicate any drifts large enough to cause a detectable change in counting rate. Tests carried out with the high-voltage supply with a voltage divider and vacuum-tube voltmeter over several days demonstrated a maximum drift of approximately 10%.

To test the effect of voltage changes on gain, the channel position of the 662-keV Cs^{137}-Ba^{137} photopeak was studied as a function of high voltage. In all cases, the relationship can be described by the following equation:

$$\Delta G/G = 7\ \Delta V/V, \qquad (2)$$

where $\Delta G/G$ is the fractional change in channel number caused by a fractional change in high voltage, $\Delta V/V$. Such a relationship is consistent with the expected seventh-power dependence of gain on high voltage.

C. Pu^{239} Production Patterns

The simplest method of determining the production patterns of Pu^{239} involves the observation of its precursor, the 2.33-day Np^{239}. This species

is a beta-gamma emitter and decays to Pu^{239m} and Pu^{239} along with the emission of various gammas.[19] Some of the gammas are strongly converted, so that X rays characteristic of plutonium are also emitted. Insofar as pulse-height analyses are concerned, the plutonium X rays appear to be the result of Np^{239} beta-gamma transitions. The actual assignment of the various X rays and gammas to Np^{239}, Pu^{239m}, and Pu^{239} is complicated and has not been established unambiguously. Any of these lines, either individually or in concert, may be used as a criterion of Np^{239} activity, since each follows from the decay of Np^{239}.

To illustrate this concept, consider an actual pulse-height analysis (see Fig. 4) of an extremely pure sample of Np^{239}, produced in this case through irradiation of depleted uranium in a vertical graphite hole of EBR-I. A rigorous decontamination from fission products and uranium was carried out in the manner described in Appendix A. The product of the decontamination consisted of approximately one millicurie of carrier-free Np^{239}. To provide the best possible conditions for spectral studies, the sample was concentrated and evaporated as a point source on a wax-covered aluminum planchet. The pulse-height analysis data, illustrated in Fig. 4, were obtained with the MTR precision pulse-height analyzer [3-in. NaI(Tl) crystal] at a source-to-detector distance of 10 cm.[20]

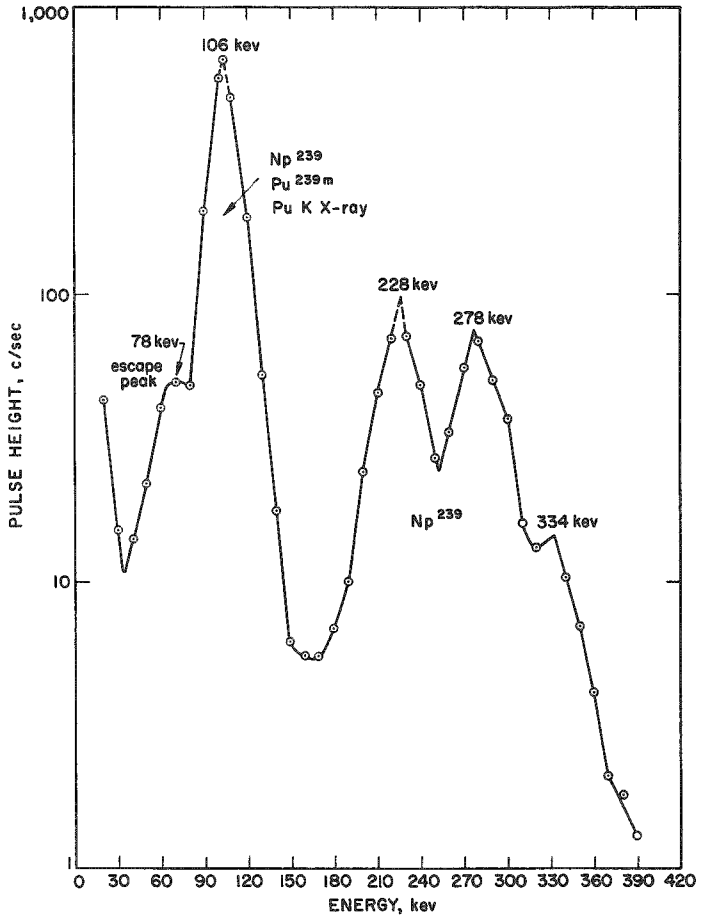

Fig. 4

Np^{239}, Carrier-free MTR Spectrometer

Figure 4 shows that the main photopeak occurs at 106 keV. This consists of contributions of gammas from Pu^{239m} and Np^{239}, and K X rays from Pu^{239}. Because each emission involves essentially the same energy, and because the resolution of the equipment is limited (approximately 16% at 106 keV), the main peak appears to be the result of a single transition at 106 keV. Each contributing line, however, is coincident with Np^{239} decay. This enables the area under the 106-keV peak to be used as a measure of Np^{239} activity.

The small 78-keV "bump" on the low-energy side of the main photopeak is the result of occasional losses of 28-keV iodine K X rays from the NaI crystal. On the high-energy side of the photopeak, three peaks occur at 228, 278, and 334 keV. These represent less strongly converted gammas resulting from beta-gamma transitions of Np^{239}.

In principle, then, it should be possible to use the intensity of any or all of these peaks as a measure of Np^{239} activity, at least on a relative basis. However, the translation of this possibility into practice is, for several reasons, not simple. Logically, an activity criterion must be established which will represent the best compromise between speed and accuracy. If time is important, it is clear from Fig. 4 that observations of the 228- and 278-keV peaks will not be as satisfactory as observations of the 106-keV peak, since statistical accuracy will suffer. It is also clear that an observation based on a single datum point taken near the center of the 106-keV photopeak is subject to the objection that small drifts in gain between successive readings could cause large errors in relative intensity measurements.

The effects of gain shifts can be lessened through the use of a technique described by Vegors et al.,[21] which is essentially based on a description of the main photopeak as a Gaussian distribution of events. With the extrapolated peak height as a measure of intensity, and the high-energy side of the photopeak as reference, a Gaussian distribution is drawn under the photopeak. An integration of the number of events occurring under the Gaussian distribution is then used as the measure of intensity. Although this technique does minimize the effects of a shift in the location of the peak, it does suffer from the following objections: the activity to be analyzed must be relatively free from interfering activities, and the method is tedious and extremely time-consuming.

A more satisfactory criterion (the one used in the measurements with Mark IV) is based on a wide-window integration of the photopeak intensity. The principle may be illustrated by considering the spectrum given in Fig. 4. The lower discriminator setting is fixed at some point on the low-energy side of the photopeak. While the exact choice of discriminator setting is somewhat arbitrary, it is important to select a setting in a region where the peak appears to be Gaussian. In Fig. 4, for example, the

lower setting could be fixed at, say, 90 keV. The window width could then be adjusted so that the intensity at the upper edge would be approximately the same as that at the lower discriminator setting. For the data of Fig. 4, this would consist of a window opening of 30 keV. Thus, all events falling in the energy band from 90 to 120 keV are integrated and registered collectively. It is clear that integration of events over a major portion of the photopeak ensures reasonable statistical accuracy. It would appear (superficially, at least) that even better statistical accuracy would result if the integration were to be carried out over an even larger portion of the photopeak, for example, from 35 to 140 keV. This, however, is not necessarily true, since the signal-to-noise ratio (i.e., the ratio of true Np^{239} events to background events) degenerates rapidly in the wings of the photopeak. Obviously, some optimum combination of discriminator and window settings exists. A narrow-band integration about the peak center ensures a high signal-to-noise ratio at the sacrifice of intensity, whereas a wide-band integration guarantees intensity at the sacrifice of signal-to-noise ratio. However, since low Np^{239} activity is not a problem in the measurements, the actual choice of settings was such that a high signal-to-noise ratio was preferred at the expense of a slight reduction in overall band intensity.

The major advantage of this approach is the relatively low sensitivity of counting rate with respect to small changes in gain. That this is true may be seen from Fig. 5, in which data in the vicinity of the 106 keV peak

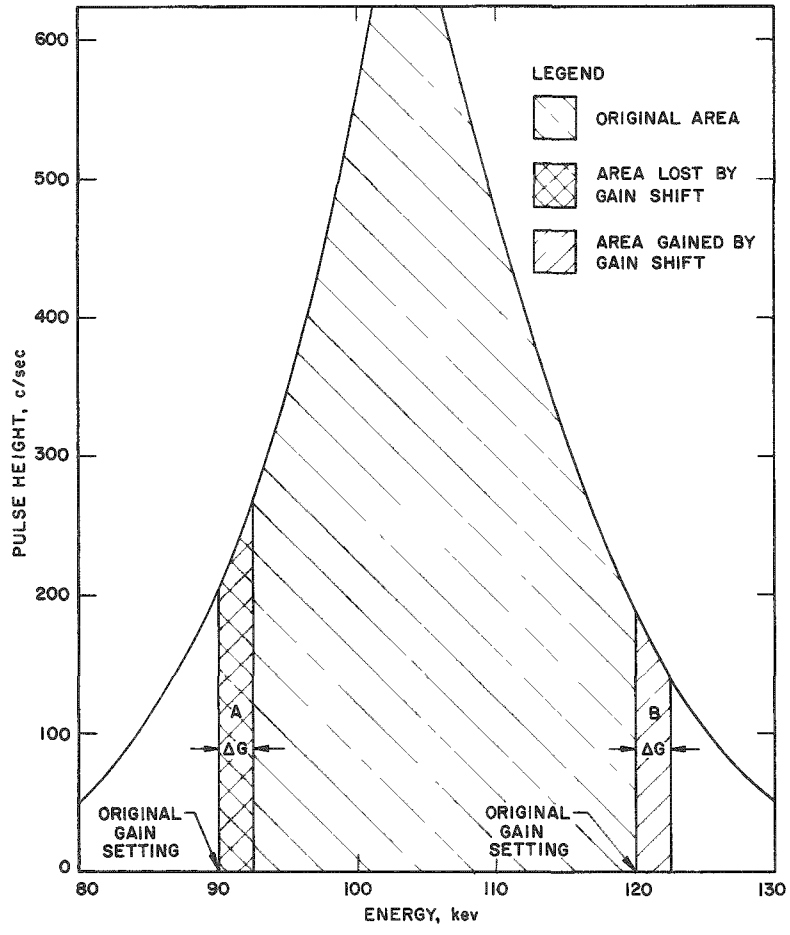

Fig. 5

Effect of Gain Shift on Intensity

(from Fig. 4) are replotted on a linear scale. The effects of a small increase in gain, ΔG, are reflected by a loss in the integrated area designated as A. The latter, however, is partially compensated by an increment, B, to the total integrated area. The net effect of the gain shift in this case is a loss of integrated area or intensity. For the case illustrated, the resultant loss is only 1.3% of the total area. However, the case illustrated must be regarded as extreme, since the fractional increase in gain used for the illustration (i.e., 2.5%) considerably exceeds the value of 0.7% expected and observed for routine operation of the equipment.

A further mitigating factor must also be considered. The effect of gain shift on the results of the Np^{239} intensity measurements is even less than the foregoing discussion would indicate. Since each observation of the 106-keV photopeak is made relative to that of a monitor foil irradiated simultaneously, the effects of gradual gain shifts (the type normally encountered) are almost entirely eliminated.

D. Background Effects

Section C above indicates that the window technique offers a reasonably reliable method for comparing intensities under the Np^{239} 106-keV photopeak. In the absence of all background effects, the precision with which the Np^{239} activity in any given foil could be compared with that of a monitor foil would be dictated exclusively by the statistical aspects of counting. In practice, background effects limit the precision and accuracy of the determinations. The following sources of extraneous radiations must be considered.

1. Environment

Background effects peculiarly associated with the area and equipment include cosmic-ray activity, radioactive contamination of the area, and electronic noise. Fortunately, the effect of all such sources, taken collectively, is relatively unimportant and is easily measured.

2. Foil

Gamma rays resulting from activities intrinsically associated with the uranium and plutonium foils constitute a sizable contribution to the noise signal. Such effects (along with environmental effects) are easily and reliably established through measurements of the activity associated with an unirradiated foil of known weight.

3. Fission Products

The largest contribution to the overall background under the 106-keV peak results from the activity of fission products produced as the

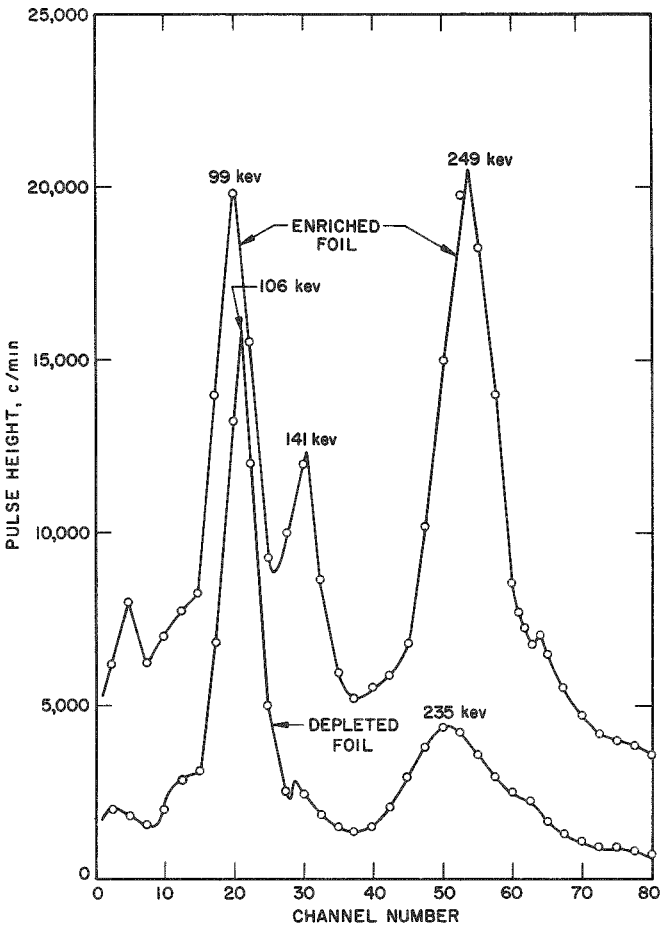

Fig. 6. Spectra of Irradiated U^{235} and U^{238} Foils

result of threshold fission in U^{238} and the fast fission of U^{235}. To obtain a measure of the importance of the fission-product effect, studies were carried out with depleted and enriched uranium foils irradiated simultaneously in the extremely hard neutron spectrum associated with the core of EBR-I. Pulse-height spectra for two foils of equal weight (one depleted and the other enriched) are shown in Fig. 6. Environmental and foil backgrounds have been subtracted in each case. Since each foil was counted for the same period of time under identical conditions of geometry, the activities can be compared directly.

The principal features of interest for the depleted-foil spectrum consist of two major peaks, one in the vicinity of 106 keV and the other in the vicinity of 235 keV. The peak near 106 keV is clearly understandable in terms of radiations intrinsically associated with Np^{239} decays. The smeared peak in the vicinity of 235 keV is almost certainly that associated with the 228- and 278-keV gammas of Np^{239}.

The spectrum of the enriched foil is characterized by three major peaks (at 99, 141, and 249 keV). Each is associated with the decay of specific fission products. The existence of peaks at 141 and 249 keV in no way jeopardizes the success of using the 106-keV photopeak as a measure of Np^{239} activity in depleted foils. The presence of the peak at 99 keV, on the other hand, is surprising since previous investigators[22] have reported that no fission product emits gammas with an energy in the vicinity of the 106-keV Np^{239} photopeak. The existence of a peak at 99 keV complicates the separation of Np^{239} from fission-product activities, since the window technique is based on an intensity integration over an energy band which of necessity includes the 99-keV peak. Although the yields of fission products from U^{235} and U^{238} are different, it must be assumed that the specific fission-product activity responsible for the 99-keV line in the irradiated U^{235} spectrum also exists in the irradiated U^{238} spectrum, even

though its effect may be obscured by more intense radiations originating from Np^{239}. A critical comparison of the two spectra of Fig. 6 indicates that the contribution of fission-product activity to the 106-keV peak intensity may be substantial.

However, because neutron fission in U^{238} is a threshold process, whereas capture is not, the relative contribution from fission products to total activity under the 106-keV peak (for irradiated depleted foils) decreases as the neutron spectrum becomes softer. It follows that corrections for fission-product effects are small in the outer blanket regions and increase rapidly toward the center of the core. An indication of the magnitude of this effect is shown in Fig. 7, in which are plotted the spectra from two depleted foils, one irradiated in the extremely hard neutron flux of AFSR[23] and the other irradiated in the relatively soft spectrum associated with the graphite region of EBR-I. For simplicity, data of both spectra have been normalized in a manner which equalizes the respective 106-keV peak intensities. These two spectra indicate that fission-product activity, essentially negligible in the thermal-neutron-activated foil, constitutes a significant fraction of the total activity in the foil irradiated in the harder spectrum. Thus corrections for fission-product effects in depleted foils irradiated in the hard neutron spectrum of EBR-I are necessary.

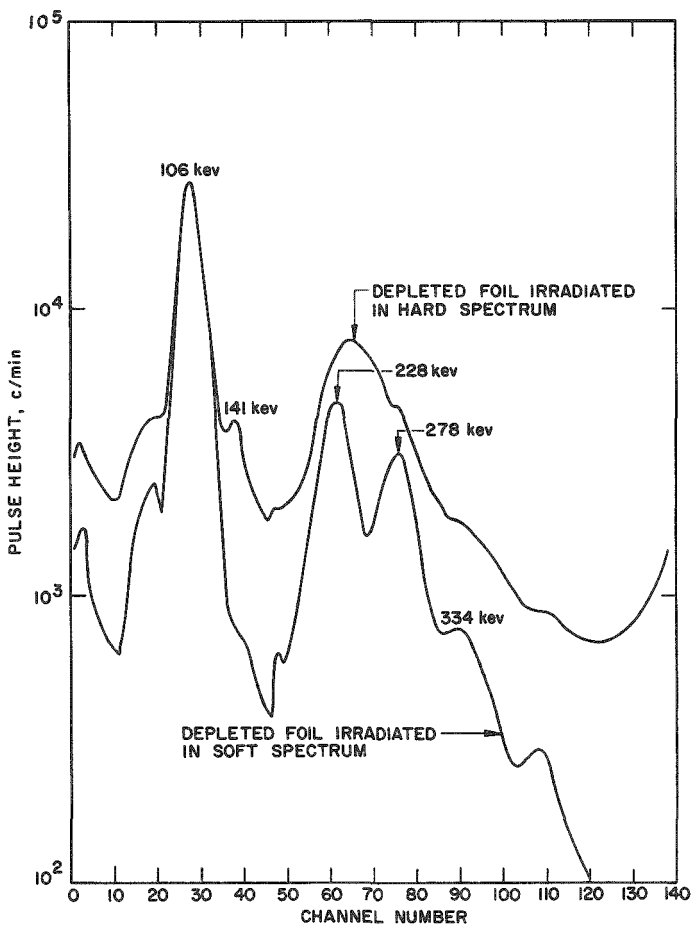

Fig. 7

Effect of Spectrum on Fission Product Generation in U^{238}

4. U^{237} Activity

Although the effects of U^{237} activity on the resolution of the Np^{239} component are expected to be small, this fact must be established experimentally. Formed by means of the threshold reaction $U^{238}(n,2n)U^{237}$, the isotope U^{237} decays with the emission of various gammas, among them two at 60 and 103 keV.[24] With the window-width settings adjusted to 87-125 keV (as eventually was the case), and with the resolution available (16% at 106 keV), it is clear that the 60-keV gamma will contribute little or nothing to the band intensity. Decays proceeding through the 103-keV emission will, however, be indistinguishable from other events falling within the band. To establish the magnitude of this effect, periodic spectrum measurements were carried out for a depleted foil irradiated under hard flux conditions at the core center of EBR-I. The results of these measurements are given in Fig. 8. Since U^{237} decays with a half-life of 6.7 days, whereas Np^{239} decays with a half-life of 2.33 days, the effect of long cooling periods tends to accent the contributions from U^{237}.

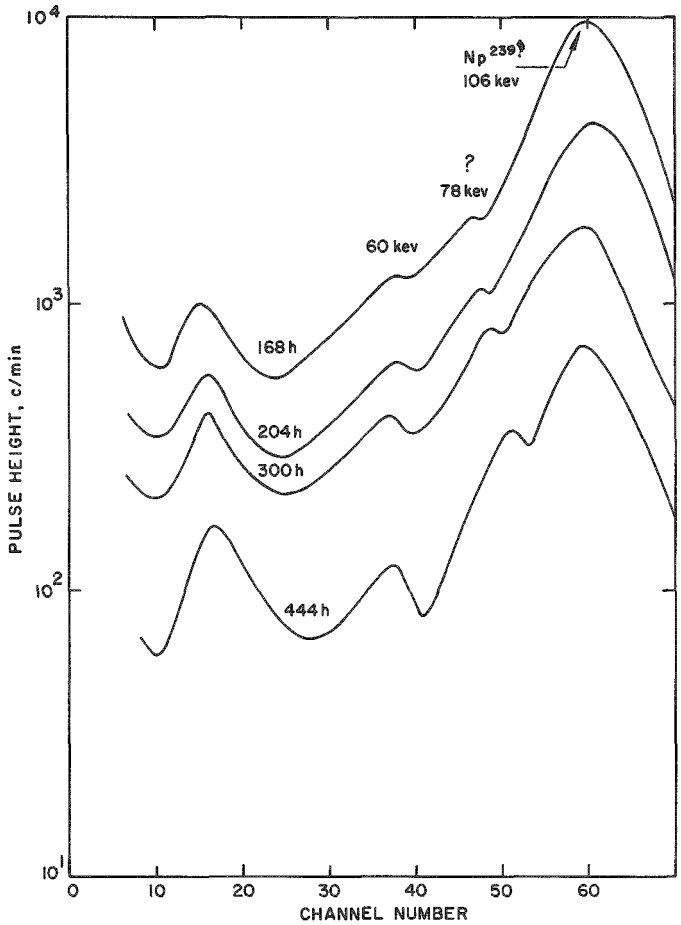

Fig. 8. U^{237} Production

For a cooling period of 168 hr, the only evidence of the 60-keV peak is a slight ripple in the spectral curve. For longer cooling periods, the ripple increases in definition until it becomes a reasonably well-resolved peak after 444 hr. Such behavior is consistent with the existence of a mixture of U^{237} and Np^{239}. For short cooling periods, the greater activity associated with the 2.33-day Np^{239} almost completely obscures the 60-keV activity. As the Np^{239} decays preferentially, the 60-keV peak becomes resolvable. This explanation, however, does not preclude the possibility that the 60-keV peak is that associated with a long-lived fission product. Nevertheless, the assignment of the 60-keV activity to U^{237} permits an evaluation of the upper limit expected for its contribution to the 87-125-keV band. Assume (1) that the integrated area under the photopeak is proportional to peak intensity, (2) that fission-product background effects may be neglected, and (3) that

the response of the detection equipment for the 60- and 103-keV U^{237} gammas is approximately the same. It may then be shown that for cooling periods of the order of 48 hr, the upper limit to the contribution from U^{237} is less than 0.7%. A contribution of this order of magnitude was considered negligible since (1) all assumptions necessary for the upper limit estimate are pessimistically imposed, (2) the amount of U^{237} produced (illustrated in Fig. 8) is abnormally high, and (3) only a small fraction of the total Np^{239} generated in EBR-I is produced in regions where U^{237} activity is significant. Accordingly, no corrections for the effects of U^{237} production were applied.

E. Separation of Np^{239} Activity from Gross Activity

Superficially, it would seem from Fig. 6 that the activity at 99 keV would entirely mask the radiations associated with Np^{239}, since the intensity of the 99-keV peak in the irradiated U^{235} spectrum exceeds that of the 106-keV peak in the irradiated U^{238} spectrum. To obtain a more realistic measure of the extent to which the 99-keV activity interferes with the resolution of the Np^{239} component, the 106-keV band for both samples can be resolved into their respective components. In this way a ratio of the true Np^{239} signal to that of fission-product noise may be obtained.

1. Estimate of the U^{235}:U^{238} Fission Ratio

A satisfactory estimate of the U^{235}:U^{238} fission ratio was obtained by comparing the relative fission-product activities associated with enriched and depleted foils irradiated under identical conditions of flux and time in the core of EBR-I. To eliminate the influence of Np^{239} radiations, the comparison was made for a spectral region considerably higher in energy than the most energetic radiation of Np^{239}. The information used for the comparison consisted of a high-energy extension of the data illustrated in Fig. 6. The results of an activity integration carried out over the region 550-710 keV were as follows: for the U^{235} foil, 75,000 c/min; for the depleted foil, 10,400 c/min. Corrections for the 6.8 w/o content of U^{238} in the enriched foil, and for the 0.22 w/o of U^{235} in the depleted foil, were carried out according to the following procedure. Defining

$$x = \text{fission product activity per mg of } U^{235}, \tag{3}$$

and

$$y = \text{fission product activity per mg of } U^{238}, \tag{4}$$

the following expressions hold:

$$I_e = w_{25}^e x + w_{28}^e y, \tag{5}$$

and

$$I_d = w_{25}^d x + w_{28}^d y, \tag{6}$$

where I_e and I_d are the integrated high-energy intensities for the enriched and depleted foils, respectively. Actual masses of U^{235} and U^{238} in the respective foils are given by w_{25} and w_{28}. From equations (5) and (6) and the measured values for the integrated high-energy counting rates, a value of 7.8 was found for the ratio x:y (i.e., for the U^{235}:U^{238} fission-product-activity ratio).

If it be assumed that the yields of fission products responsible for the fission-product activity under the 106-keV peak are the same for both U^{235} and U^{238}, the fission-product intensity under the peak may be approximated in the following manner. Defining

u = fission product activity per mg of U^{235} (under the 106-keV peak),

v = fission product activity per mg of U^{238} (under the 106-keV peak),

and

z = the Np^{239} activity per mg of U^{238} (under the 106-keV peak),

where u/v = 7.8, it is possible to set up the following simultaneous equations, where equation (7) refers to the data from the irradiated enriched foil and equation (8) refers to data from the irradiated depleted foil:

$$I_e = w_{25}^e u + w_{28}^e v + w_{28}^e z, \tag{7}$$

and

$$I_d = w_{25}^d u + w_{28}^d v - w_{28}^d z. \tag{8}$$

Here e and d designate the enriched and depleted foils, respectively, and w_{25} and w_{28} are defined as the actual masses of U^{235} and U^{238} in the respective foils. From an integration of the peak intensities over the energy range included between channels 15 and 25 (see Fig. 6), values of 67,000 and 40,000 c/min were found for I_e and I_d, respectively. Substitution of these values into equations (7) and (8) and the use of 7.8 for the ratio u:v resulted in a value of 3.71 for the ratio z:y, which is the ratio of capture to fission-product activity in U^{238} for the conditions specified. A capture-to-fission ratio determined in this manner is sensitive to the time elapsed between the end of the irradiation and the time of counting. However, the value 3.71 corresponds to an "out-of-pile" time of 48 hr, approximately the time required to give maximum discrimination against fission-product activities. It follows, then, that for waiting periods of the order of 48 hr, approximately 21% of the total activity associated with the 106-keV photopeak originates from various fission products. Clearly, a contribution of this magnitude must be considered in the separation of the Np^{239} component from the total response of the 106-keV band. However, since the depleted foil was irradiated in an extremely hard neutron spectrum (that associated with the core of EBR-I),

the deduced value of 21% may be regarded as a realistic estimate of the upper limit of the fast-fission-product background effect. For depleted foils irradiated in the outer regions of the blanket, where the neutron spectrum is considerably softer, it follows that the fission-product component will be much less important.

2. Method for Estimating the Fission Product Background

Although the discussion above points out the fission-product problem and leads to a method of estimating the fission-product contribution, a more accurate method must be applied. In the first place, the above treatment is premised on the unjustifiable assumption that the yields of the interfering fission-product activities are the same for fissions in both U^{235} and U^{238}. In the second place, the partition of integrated peak intensity between Np^{239} and fission-product activities is sensitive to time, since it is known that the 99-keV component prominent in the U^{235} fission-product spectrum decays with a half-life significantly longer than that of Np^{239}. Accordingly, it was necessary to develop a more accurate and more reliable technique, one which is unaffected by the difference in U^{235} and U^{238} fission-product yields and which is also insensitive to the time elapsed after the irradiation.

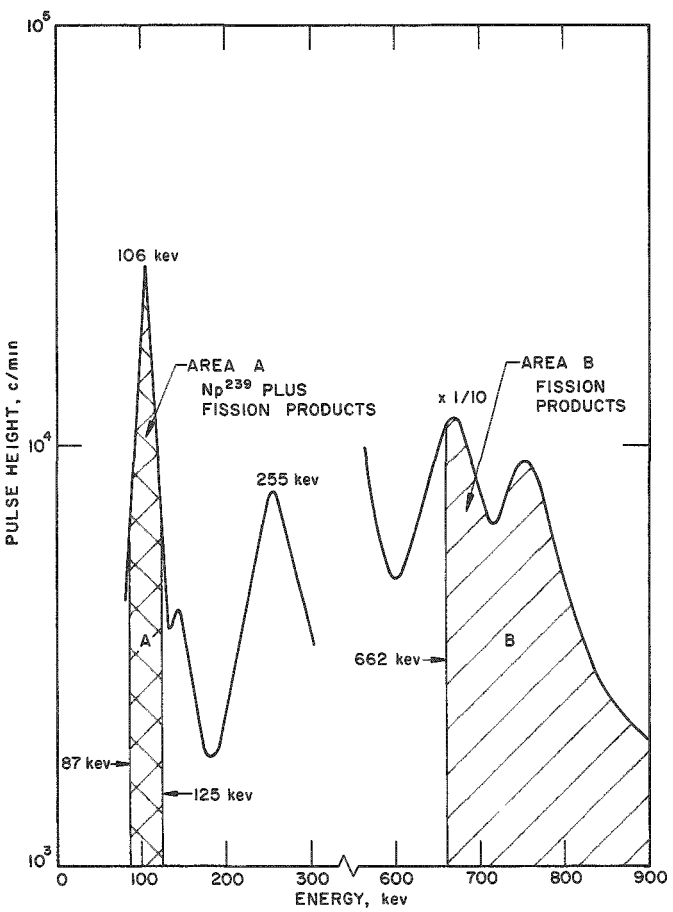

Fig. 9. Definition of Bands A and B

The technique developed for the measurement of fission-product activity under the 106-keV peak is based on an experimental measurement of the ratio of fission-product activity in a fixed high-energy band, where Np^{239} activity is missing, to that in a fixed low-energy band which "straddles" the Np^{239} photopeak. This concept is illustrated in Fig. 9, which gives the gamma spectrum associated with a depleted foil irradiated in a hard neutron spectrum. Two specific bands are labeled. One, designated as Band A, includes the total (integrated) response over the energy region from 87 to 125 keV; the other, designated as Band B, includes the integrated response of all events having an energy greater than 662 keV (an energy selected to coincide with the photopeak from a Cs^{137}-Ba^{137} calibrating source). All events

in Band B are the result of gamma transitions from fission products formed in the threshold fission of U^{238}. Events in Band A include: (1) Np^{239} and Pu^{239m} gammas, and Pu^{239} K X rays; (2) fission-product gammas; and (3) uranium K X rays originating from the conversion of fission-product gammas in the uranium matrix of the foil. The first of these is, of course, the signal of interest. That a portion of the signal arises from Pu K X rays is of little significance, since the X rays are, in this case, the result of internal conversion during Np^{239} decay. Since the emission of Pu K X rays coincides with the decay of Np^{239}, the response of the detection equipment is proportional to the gross Np^{239} activity.

With the limited resolution afforded by the detection equipment, radiations emitted as the result of Np^{239} decays cannot be distinguished from uranium K X rays and from those associated with the various fission-product activities. Fortunately, the background effects of uranium K X rays and fission-product gammas do not need to be separated into individual components. Uranium K X rays are formed as the result of conversion in the uranium matrix of soft gammas emitted in the decay of various fission products. Since the intensity of the uranium K X rays is directly proportional to the gross fission-product activity, the X rays and fission-product gammas may be regarded as a single inseparable background component. The problem, then, is one of separating the gross Band A intensity into two components, one originating from decays in Np^{239} and the other originating from fission-product activity (after a suitable background correction for environmental effects).

Logically, it would seem that if the ratio of fission-product activity in Band B to that in Band A could be established as a function of time, the fission-product response in Band A could be evaluated from that measured in Band B. However, the establishment of this ratio is not simple. Superficially, it would appear that such a measurement could be conducted with a sample of separated U^{238} fission products. Although this could be done, the results obtained would neglect several effects which have a direct bearing on the accuracy of separating the Band A fission-product component. The primary objection is concerned with the origin of uranium K X rays. In the traverse foils, the K X-ray component is proportional not only to the fission-product activity, but also to the mass of uranium in the foil. In a perfectly separated sample of U^{238} fission products, uranium would be missing and the effective fission-product response in Band A would be underestimated by the uranium K X-ray component. Attempts to measure the K X-ray component by covering the separated fission-product sample with a uranium foil would be subject to the following objections: (1) the uranium foils would attenuate fission-product gammas; and (2) the effects of nondispersion of the fission products uniformly throughout the foil would be difficult to assess. It is essential, then, to evaluate the combined effects of fission products and uranium K X rays from studies carried out with foils identical, or at least as nearly identical as possible, to those

actually used in the traverse measurements. The advantage of such an approach is that corrections for attenuation effects of fission product gammas in the foil and for the production of uranium K X rays may be avoided.

The calibration cannot be carried out directly with a depleted foil, since the overriding intensity of the Np^{239} component would completely mask that associated with fission products. Rather, the calibration must be carried out with a set of two foils (one depleted and one enriched) which have been subjected to identical irradiation conditions. In this way, corrections can be made for the effects of Np^{239} produced in the enriched foil and for the effects of U^{235} fission products generated in the depleted foil. This approach is premised on the assumption that the Band B:Band A fission-product activity ratio is the same for both U^{238} and U^{235} isotopes. For out-of-pile times longer than 35 hr, it will be shown that this assumption is valid.

Data pertinent to an evaluation of the B:A ratio were obtained by means of a single-channel analyzer (see Section IV-B above) from enriched and depleted foils irradiated simultaneously at the center of the Mark IV core. As illustrated in Fig. 9, gain and discriminator settings were adjusted so that Band A registered those events between 87 and 125 keV, while Band B registered total events with energies greater than 662 keV. The spectrometer with the 662-keV photopeak of a Cs^{137}-Ba^{137} source was calibrated periodically to eliminate the effects of small changes in gain. The counting results are summarized in Table I. In all cases, corrections have been applied for foil and environmental background. The results in Table I indicate that the B:A ratio for any given out-of-pile time is greater for the enriched foil. This, of course, is the result of the much greater contribution to Band A from Np^{239} activity in the depleted foil.

To evaluate B:A from the information of Table I, corrections must be applied for the effects of the 6.8 w/o of U^{238} in the enriched foil and for the effects of the 0.22 w/o of U^{235} in the depleted foil. Such corrections were carried out in the manner described in Section IV-E-1.

Assuming that the U^{235}:U^{238} fission-product-activity ratio, x:y, determined from Band B counting data (for both foils) holds also for Band A (i.e., x:y = u:v), equations (7) and (8) may be reduced to two simultaneous equations in two unknowns. In this way, each of the parameters, u, v, and z may be evaluated. These values are summarized as a function of time in Table II. Subtraction of the Np^{239} activity in the enriched foil (see Table II, column 6) from the Band A enriched-foil net activity (see Table I, column 2) gives the net fission-product activity (see Table II, column 7) in Band A for the enriched foil. Division of the enriched-foil Band B activity (see Table I, column 3) by the corrected enriched-foil Band A fission-product response (see Table II, column 7) gives the value for B:A listed in column 8 of Table II. Contributions from U^{238} fission products in the enriched foil Band B

Table I

SUMMARY OF BAND A AND BAND B COUNTING DATA

(1)	(2)	(3)	(4)	(5)
Time after Shutdown (hr)	Enriched Foil*		Depleted Foil**	
	Band A Net (c/min)†	Band B Net (c/min)†	Band A Net (c/min)†	Band B Net (c/min)†
29.2	113,816	107,760	61,234	14,413
30.2	109,707	104,160	60,582	13,819
32.1	101,995	93,313	58,718	12,325
34.3	94,378	83,866	55,776	11,247
36.8	87,377	70,735	53,855	9,340
40.2	79,133	59,019	50,838	7,873
43.4	72,014	49,971	48,050	6,794
48.3	64,252	45,254	45,279	6,202
50.4	60,399	41,344	43,305	5,744
52.7	57,678	39,102	42,396	5,485
54.6	55,097	36,950	41,016	5,184
70.6	40,918	24,202	33,381	3,499
73.7	39,093	23,568	32,018	3,393
75.4	38,039	22,534	31,589	3,375
78.2	36,022	21,875	30,138	3,216
95.4	29,124	16,656	24,594	2,425
101.6	27,325	15,656	22,815	2,381

*Mass of 50.5 mg.

**Mass of 48.7 mg.

†Corrections for room and foil background have been applied.

Table II

EVALUATION OF B:A RATIO

(1)	(2)	(3)	(4)	(5)	(6)	(7)	(8)
Time after Shutdown (hr)	x	y	x/y	z	U^{238} Capt. Activity Enriched Foil (kc/min)	U^{235} F.P. Activity Enriched Foil (kc/min)	B:A
	U^{235} F.P. Activity per mg, Band B (kc/min)	U^{238} F.P. Activity per mg, Band B (c/min)	(Smoothed)	U^{238} Capt. Activity per mg, Band A (c/min)			
29.2	2.27	292	7.78	961	3.30	111	0.975
30.2	2.21	279	7.91	957	3.29	106	0.979
32.1	1.96	249	7.87	939	3.22	98.8	0.945
34.3	1.77	228	7.76	897	3.08	91.3	0.918
36.8	1.49	189	7.88	875	3.00	84.3	0.838
40.2	1.24	159	7.80	834	2.86	76.3	0.774
43.4	1.050	138	7.64	795	2.73	69.3	0.721
48.3	0.953	126	7.60	762	2.62	59.6	0.759
50.4	0.869	116.3	7.47	725	2.49	57.9	0.713
52.7	0.823	111.1	7.41	713	2.45	55.2	0.708
54.6	0.763	105.0	7.26	692	2.38	52.7	0.701
70.6	0.511	70.9	7.21	570	1.958	39.0	0.621
73.7	0.497	68.7	7.23	546	1.876	37.2	0.633
75.4	0.474	68.4	6.93	540	1.856	36.2	0.623
78.2	0.459	65.2	7.05	534	1.834	34.2	0.639
95.4	0.351	49.1	7.15	420	1.444	27.7	0.601
101.6	0.376	29.1	6.85	389	1.335	26.0	0.602

counting rate may be neglected as insignificantly small. Values of B:A as a function of time are plotted in Fig. 10. As expected, the ratio decreases with increasing time as the more energetic gammas associated with the shorter-lived fission products preferentially decay.

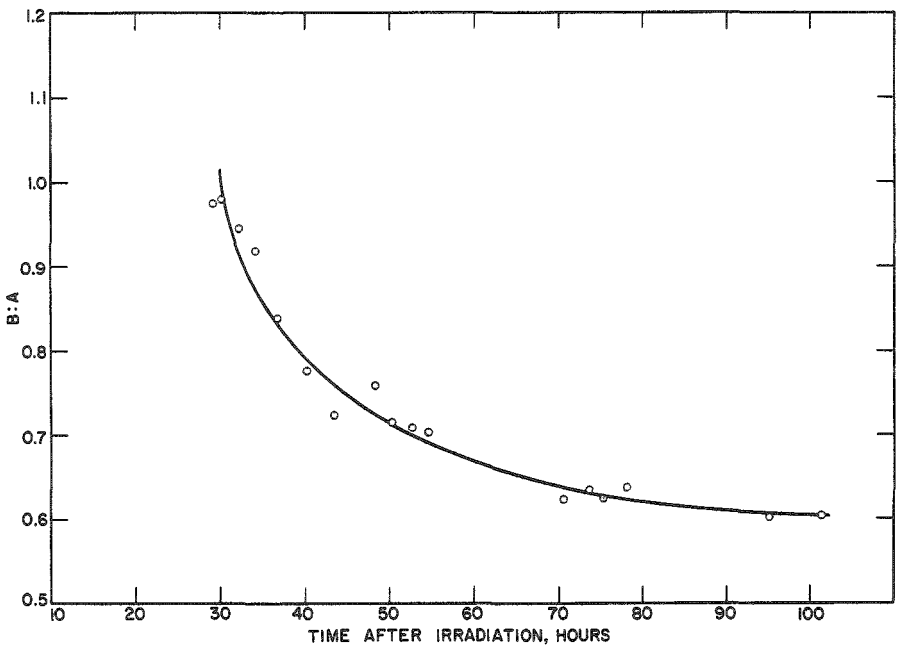

Fig. 10. B:A Ratio (Metallic Foils)

Alternatively, the depleted-foil Band A counting rate may be corrected for Np^{239} activity, and the ratio B:A may be determined directly from the counting data obtained with the depleted foil. However, the poorer counting statistics associated with the depleted-foil Band B counting rate effects a somewhat less precise evaluation of B:A. It will be shown that for out-of-pile times longer than 35 hr, values of B:A are the same for both U^{235} and U^{238} fission products.

3. Measurement of the B:A Ratio for Separated Fission Products

To prove that the B:A ratio is essentially the same for fission products, irrespective of their origin, it was necessary to carry out measurements with separated fission products. Two foils, one enriched and one depleted, were irradiated simultaneously in the Glory Hole of AFSR.[23] After a wait-time of approximately 5 hr, the samples were processed radiochemically for Np^{239}, as outlined in Appendix A. (A wait-time is necessary to ensure that all, or nearly all, of the various Kr and Xe fission products have decayed to nonvolatile chemical species. Immediate dissolution of the metallic foils would have led to a serious loss of these fission products and their respective daughters.) This procedure resulted in two fractions, one consisting of Np^{239}, the other consisting of uranium, various carrier materials, and fission products. To ensure a complete decontamination from

Np^{239}, the fission-product fraction was subjected to a second decontamination cycle. A portion of the doubly purified fission-product fraction was transferred and evaporated onto a platinum planchet. To correct for background effects arising from the various activities associated with the U^{238} decay chain, the yield of the transferred sample had to be evaluated. If it be assumed that no disproportionation of uranium, daughters, and fission products occurred in the transfer, the yield may be evaluated by comparing the gross responses of the fission-product fraction with that from an identical and unprocessed depleted foil irradiated under the same conditions of time and power. To avoid complications from Np^{239}, counting operations were carried out in Band B with the system biased at 662 keV. In this way, the yield of the fission-product sample was established as 26%.

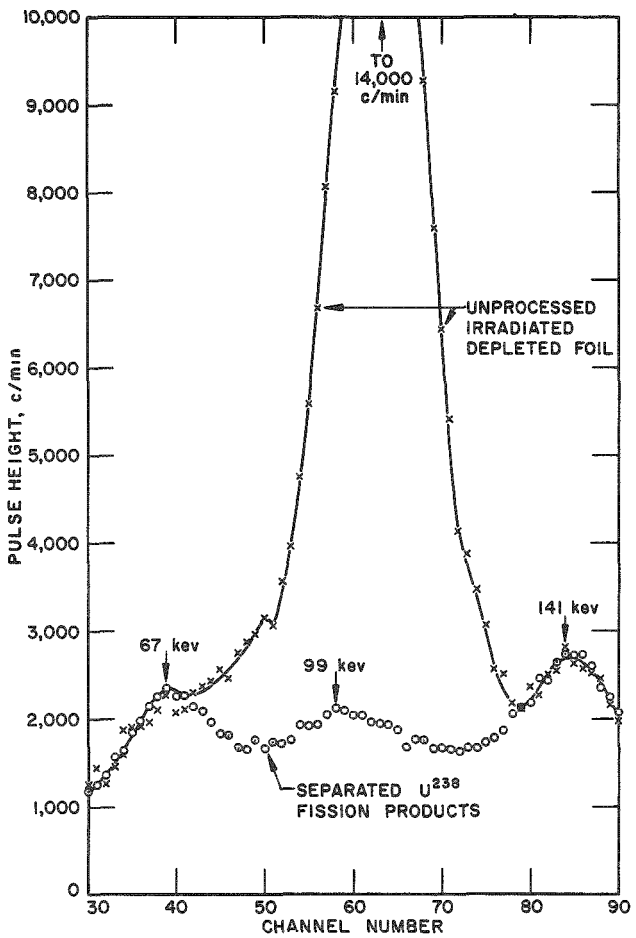

Fig. 11. Spectra of Processed and Unprocessed Irradiated Depleted Foils

A measure of the success of the decontamination of U^{238} fission products from Np^{239} may be inferred from Fig. 11, which compares the spectra from processed and unprocessed irradiated depleted foils over the region from 50 to 150 keV. To account for losses in the fission-product separation and subsequent transferral operations, the data for the fission-product fraction have been normalized to the unprocessed foil data in the region of channels 30-35. Figure 11 indicates that the spectral curve for the separated fission products is characterized by small, highly smeared peaks in the vicinity of 67, 99, and 141 keV. No attempt was made to explain the origins of these peaks in terms of specific fission products.

The most important feature characterizing the separated U^{238} fission product spectrum is the complete lack of evidence for a peak in the vicinity of 106 keV. Clearly, all or nearly all of the Np^{239} was removed from the sample through the radiochemical operations. The spectrum of the unprocessed depleted foil, on the other hand, is characterized by an

extremely well-defined peak at 106 keV. These results indicate that the separated U^{238} fission-product sample was essentially free of Np^{239}. The results further emphasized the sizable contribution to total activity made by fission products under the 106-keV peak.

Parallel studies carried out with a pair of irradiated enriched foils, one unprocessed and the other processed radiochemically, verified the complete removal of Np^{239} formed in the 6.8% abundant U^{238} isotope.

The results of B:A measurements conducted with the separated fission product samples are summarized in Fig. 12. For times between 0 and 30 hr after an irradiation, the B:A values for U^{238} fission products lie consistently above those for U^{235}. For wait-times greater than 35 hr, the curves meet and become indistinguishable within the limits of experimental accuracy.

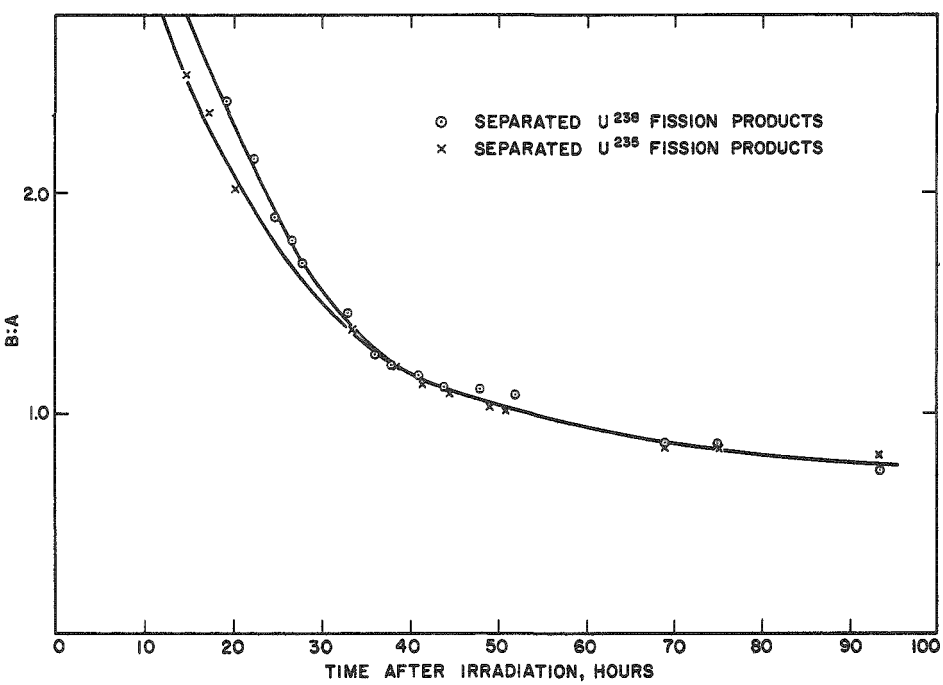

Fig. 12. B:A Ratio for Separated Fission-product Samples

Figure 10, in which values of B:A are plotted as a function of time for measurements conducted with a metallic foil, shows values substantially less than those established from the separated fission-product samples. Such a disagreement is not surprising, since the ratios were obtained under drastically different conditions of geometry and sample thickness. The results of measurements conducted with the separated fission products would be expected to yield higher values of B:A, since the softer gammas in Band A would be preferentially attenuated in the more massive sample resulting from the carrier chemical operations. The fact that values of B:A depend on the matrix in which the fission products

are embedded points out the necessity for carrying out the calibration with foils of size, shape, and thickness identical with those used in the actual traverse measurements. The results of Fig. 12 indicate that the calibration may be used interchangeably for enriched and depleted foils, within the restriction that waiting-times exceed 35 hr.

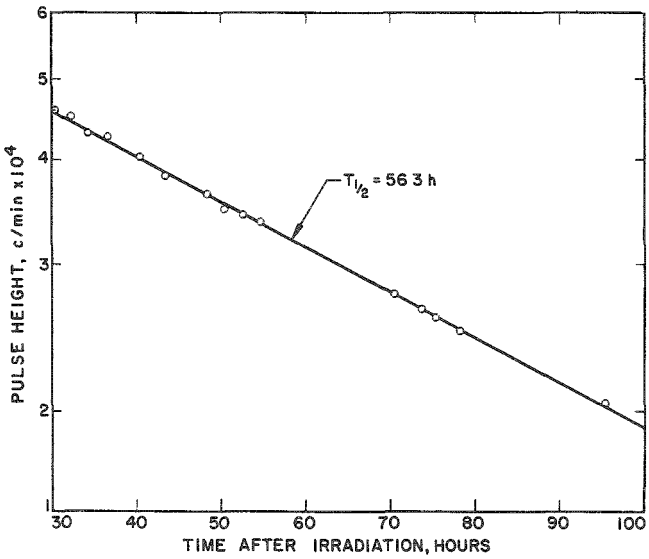

Fig. 13. Separation of Np^{239} Component from Depleted Foil Irradiated at Core Center

Figure 13 indicates that the Np^{239} component can be separated accurately from gross fission products generated through a hard-spectrum irradiation of depleted uranium. In this case, the foil was irradiated at the center of the Mark-IV core. Over a period from 30 to 100 hr after the irradiation, the Band A and Band B intensities were measured with the single-channel analyzer. From the Band B counting rate and the measured value of B:A taken from Fig. 10, the fission-product contribution in Band A was evaluated. The difference between the gross Band A counting rate (after appropriate background subtractions) and the estimated fission-product contribution gave the Np^{239} values plotted in Fig. 13.

Within limits of experimental accuracy, the Np^{239} component was found to decay with a half-life of 56.3 hr, in excellent agreement with the commonly accepted value of 56.3 hr.[19] Although the half-life test is not, by itself, definitive, it is clear that if B:A is overestimated, the half-life measured for the Np^{239} component would be too long. Conversely, if the B:A ratio were to be underestimated, the Np^{239} component would decay with a half-life shorter than the accepted value. As discussed in Appendix B, relatively large errors in values established for the B:A ratio have little effect on the integrated plutonium production throughout the system.

4. Choice of Window Settings for Band A

As discussed in Section IV-C, the actual choice of window settings (i.e., low-energy base line and window width) is somewhat arbitrary, in that many combinations of these settings could be used with little effect on the statistical accuracy of the separated Np^{239} component. Figure 14 presents the results of measurements conducted for the region of the 106-keV Np^{239} photopeak in which the window width was studied parametrically as a function of low-energy base-line settings. Window widths

of 5, 4, and 3 V were tried, corresponding, respectively, to 38, 30, and 23 keV. Figure 14 indicates that as the window width increases (i.e., as the band width becomes larger), the intensity increases and the maximum in the intensity curve shifts to lower base-line settings. A strong tendency for the intensity maximum to converge as the window width increases may also be seen. Such behavior means essentially that little benefit results from additional increases in window width. Accordingly, the settings established for Band A were a base-line setting of 11.5 V and a window width of 5.0 V. With these settings, all events between 87 and 125 keV were integrated and registered by the counting equipment. That this choice of settings effectively straddles the 106-keV photopeak is evident from the pulse-height data of Fig. 9.

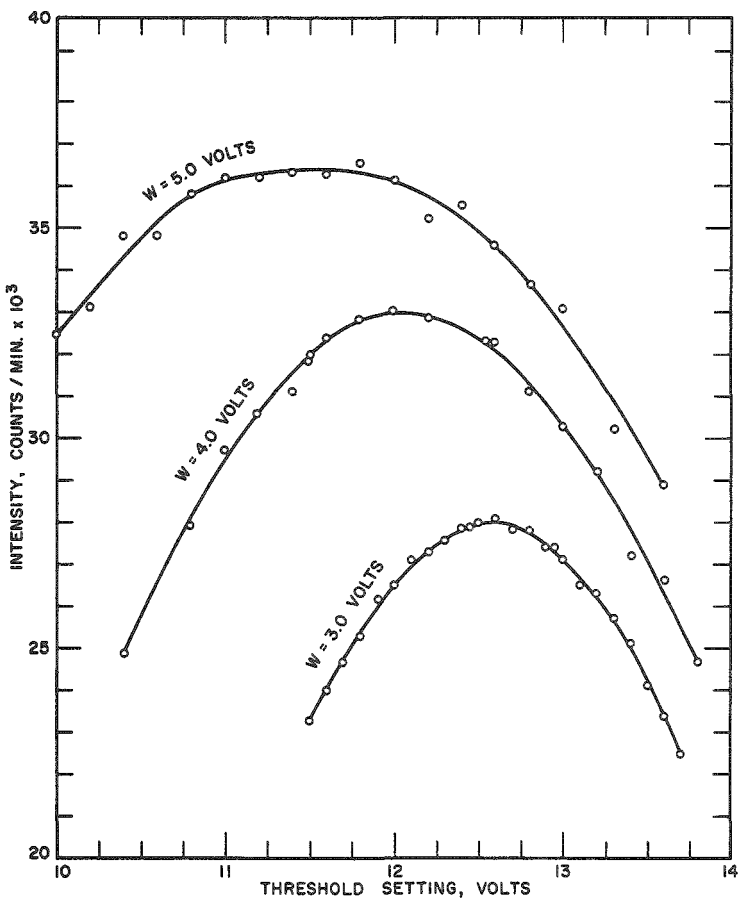

Fig. 14

Effect of Window Width on Intensity

F. Irradiations

1. Baskets and Slugs

To preserve the physical composition and nuclear characteristics of the reactor to as large an extent as possible, all foil irradiations conducted in the core and inner blanket were carried out with the foils inserted between slugs. In the light radial breeding blankets, metallic slugs of depleted uranium were used; in the fuel region, the foils were inserted

between slugs of aluminum-clad fuel-grade plutonium. In the outer blanket (cup), the foils were inserted in depressions milled in a depleted uranium sheet, which in turn was inserted vertically between two columns of blanket bricks.

To facilitate loading operations for core and inner-blanket irradiation studies, the foils, along with appropriate slugs, were loaded into stainless steel baskets, each equipped with a screw-eye for lifting. The baskets were lowered by means of iron wire to the bottom of blind thimbles inserted at various locations throughout the core and inner blanket. The various thimble locations are identified in Fig. 15. The positions and distances of the various thimbles from core center are listed in Table III.

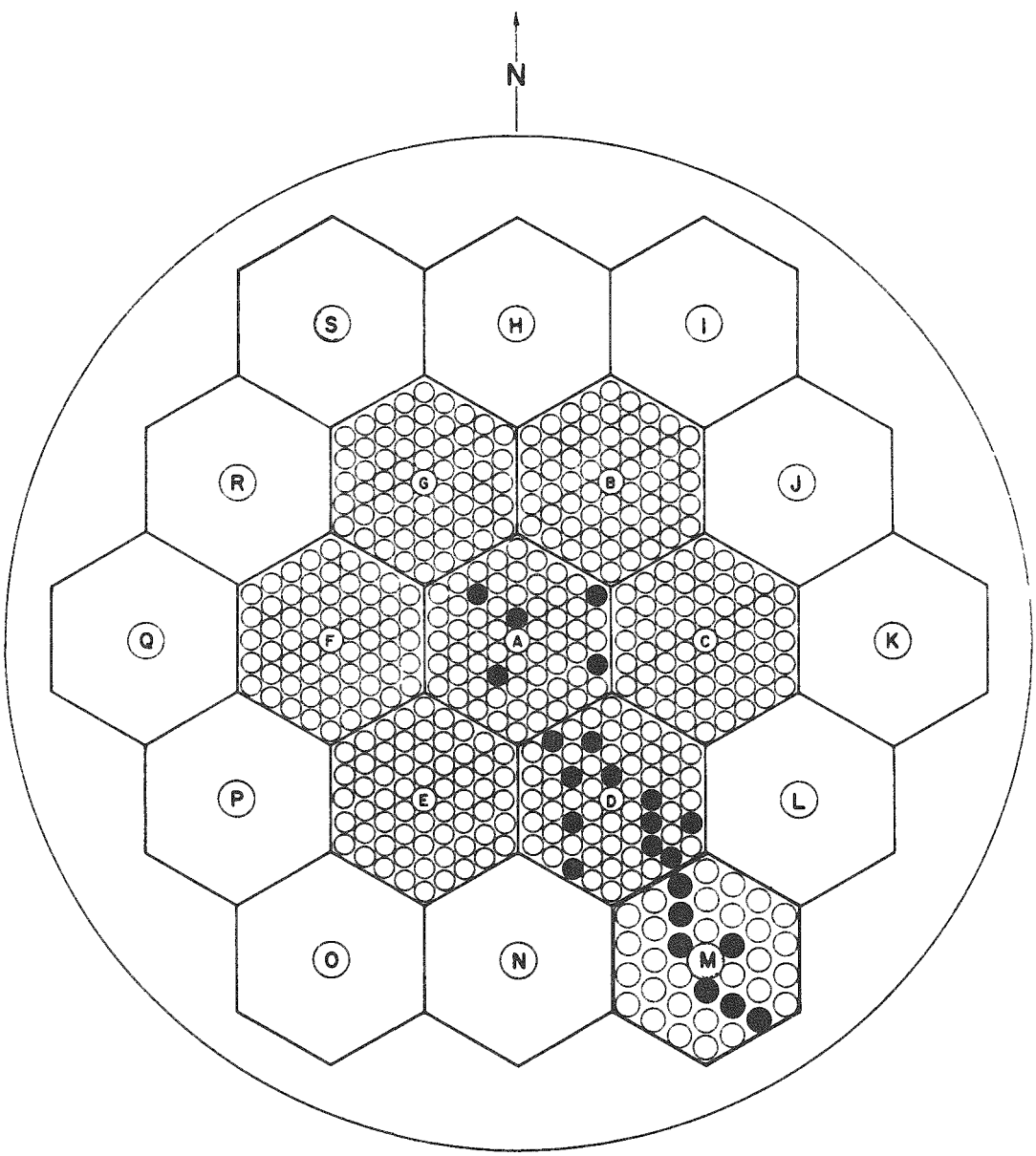

Fig. 15. Thimble Positions in EBR-I, Mark IV

Table III

THIMBLE POSITIONS

Rod Location	Distance from Core Center (in.)	Rod Location	Distance from Core Center (in.)
A-30	0.348	D-18	3.637
A-24	0.613	D-49	3.800
A-13	0.938	D-60	4.089
A-60	1.281	D-56	4.113
A-57	1.392	M-10	4.525
D-6	1.688	M-11	4.927
D-20	1.950	M-12	5.313
D-14	2.262	M-24	5.718
D-30	2.563	M-19	6.094
D-16	2.938	M-26	6.438
D-47	3.218	M-32	6.885
D-48	3.488		

2. Enriched Foils

All enriched foils used in the traverses consisted of metallic uranium discs, 0.200 in. in diameter and 0.005 in. thick. An isotopic analysis gave the following values: U^{235}, 93.2 w/o; U^{238}, 6.8 w/o. Irradiations were conducted throughout the various inner-blanket regions at approximately one-in. increments of elevation. In the massive outer blanket (cup), irradiations were conducted at 1.5-in. vertical and 0.5-in. radial increments. No irradiations were conducted in the core, since the fuel material was exclusively plutonium.

3. Depleted Foils

The depleted foils were also in the form of metallic discs, 0.200 in. in diameter and 0.005 in. thick. An isotopic analysis gave U^{238}, 99.78 w/o; U^{235}, 0.22 w/o. The masses of typical depleted and enriched foils were approximately 50 mg. To simplify problems of data reduction, the depleted foils were irradiated at the same vertical and radial coordinates as for the enriched foils.

4. Plutonium Foils

All plutonium foils consisted of thin discs of Pu-1.25 w/o aluminum alloy, clad with approximately 6 mils of aluminum, pressed and cold-welded along the periphery. The "meat" consisted of a disc 0.150 in. in diameter and approximately 0.003 in. thick. Before cladding, the mass of each disc (approximately 15 mg) was established with a precision of ± 5 μg with a microbalance. An isotopic analysis gave, in w/o, Pu^{238}, 0.01; Pu^{239}, 94.91; Pu^{240}, 4.60; Pu^{241}, 0.48.

Irradiations were carried out at approximately one-in. increments of elevation at ten different radial positions in the core. No plutonium irradiations were carried out in the blankets, since the plutonium concentration in the blanket regions was insignificantly small.

A vertical cross section through the reactor, shown in Fig. 16, indicates the various regions and their dimensions. The composition of each region is specified in Table IV. It follows from Fig. 16 that a typical fuel-rod traverse involved the simulation of the lower 3.552 in. of blanket, the 8.484-in. plutonium core, and the upper 7.745-in. blanket. For typical Mark-III and Mark-IV blanket-rod traverses, however, the baskets were filled exclusively with blanket material.

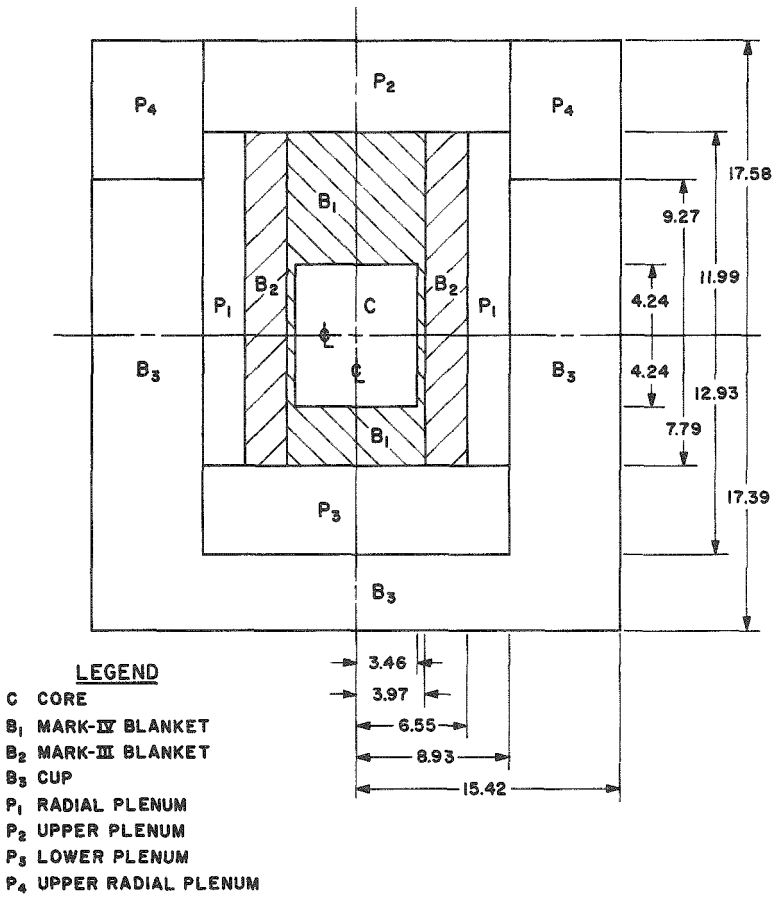

Fig. 16

Mark-IV Loading
(dimensions in in.)

Table IV

MARK-IV CORE AND BLANKET COMPOSITION
(See Fig. 16)

Region	Composition (v/o)
C, Core	304 SS, 6.3; Al bronze, 0.5; Zircaloy-2, 21.1; NaK, 36.7; Pu, 35.3
B_1, Mark-IV Blanket	304 SS, 6.3; Al bronze, 0.5; Zircaloy-2, 21.1; NaK, 36.6; depleted U, 35.4
B_2, Mark-III Blanket	304 SS, 7.3; NaK, 25.6; natural U, 48.9; Zr, 18.2
B_3, Cup	304 SS, 4.36; natural U, 85.1
P_1, Radial Plenum	304 SS, 54.1; Al, 5.44; NaK, 12.97; Inconel, 2.84
P_2, Upper Plenum	304 SS, 71.5; NaK, 22.2
P_3, Lower Plenum	304 SS, 27.1; Al, 4.91; NaK, 35.4; Inconel, 2.21; Zr, 3.45
P_4, Upper Radial Plenum	304 SS, 75

Approximately 18 hr after an irradiation, the baskets were removed from the thimbles and opened with a tubing cutter. The foils were removed for subsequent counting operations. To minimize the hazards associated with the accidental release of plutonium from faulty slugs or foils, all loading and unloading operations of fuel baskets were carried out in a hood specifically designed for plutonium handling.

5. Summary of Irradiations

Since it was impractical to irradiate all foils simultaneously, a series of individual runs was conducted. The various runs, along with other pertinent information, are summarized in Table V.

Table V

SUMMARY OF RUNS

Run No.	Type of Foil Used	Region	Power Level (kW)	Irradiation Time (min)
1	Plutonium and enriched	Core and upper and lower Mark-IV blankets	1	15
2	Depleted	Upper and lower Mark-IV blankets	1	15
3	Depleted	Mark-III and Mark-IV blankets	5	15
4	Enriched	Mark-III and Mark-IV blankets	2	15
5	Depleted	Cup	5	15
6	Enriched	Cup	2	15
7	Enriched	Cup	2	15
8	Depleted	Cup	5	15

As discussed in Section G below, corrections for the difference in power between individual runs are made unnecessary by a data normalization.

G. Counting

1. Plutonium and Enriched Uranium Foils

Counting operations for both types of foil (i.e., plutonium and enriched uranium) were carried out with the single-channel analyzer described in Section IV-B. For these foils, the measure of fission-product activity was the intensity registered in Band B, i.e., gain and discriminator settings were adjusted so that only those events having energies greater than 662 keV were registered. The spectrometer was calibrated periodically with a Cs^{137}-Ba^{137} source to minimize the effects of small changes in

gain. Occasional drifts in gain, evidenced by shifts in the position of the 662-keV photopeak, were compensated by changes in the high voltage supplied to the photomultiplier tube. Without exception, the few changes noted throughout the various measurements were small. The foils were counted under rigidly controlled conditions of geometry. Each was placed in a small circular depression milled in a tray, which in turn fitted accurately into a slotted castle-type tray holder.

Since many foils (usually 100-150) were involved in a single traverse, corrections for decay occurring between the beginning and the end of a counting sequence were necessary. To simplify the corrections, the activity of a monitor foil, irradiated simultaneously, was measured periodically. A plot of the activity as a function of time gave a smooth curve which was used to obtain an extrapolated value for the monitor activity at any given time. Division of the activity of any given traverse foil by that of the monitor for the same time gave (after a weight normalization) the number of fission events per unit fission event in the monitor foil.

2. Depleted Foils

All counting operations were conducted with the single-channel analyzer described previously. Two counts per foil were taken: one in Band A (87-125 keV), the other in Band B ($\nearrow$662 keV). Periodic observations of the activities of a simultaneously irradiated depleted monitor foil in both Bands A and B were taken to permit a common normalization of all depleted traverse foils. Band B information was used for the evaluation of the fission-product component in Band A and for an evaluation of the fast-fission effect. Band A information was used for an evaluation of the Np^{239} activity.

3. Monitoring Locations

Enriched uranium monitor foils were irradiated at a fixed reproducible position in a probe which penetrated to a fixed location in one of the vertical graphite holes. Plutonium monitoring foils were located at a fixed position close to the center of the core. Depleted uranium monitor foils were irradiated at a fixed position along the core-upper blanket interface.

4. Background Corrections

As discussed in Section IV-D, background corrections were established by counting corresponding unirradiated foils under identical conditions of geometry. In this way, corrections for the effects of activities intrinsically associated with the foil materials, as well as environmental effects, were established through a single measurement. On occasion, the practical necessity of locating the foil-holding tray near the counting equipment introduced a background component which decayed with time. For situations in which the effect was measurable, periodic measurements plotted as a function of time permitted a decay correction.

H. Foil Traverse Data

1. Plutonium Fission Distribution

The organization of counting data into a logical and practical form for integration involved the following operations (not necessarily consecutive).

a. Every 30 min, the Band B (fission product) counting rate was measured for the aluminum-clad plutonium monitor foil. Subtraction of experimentally measured values for environmental and unirradiated foil background from the gross counting rate resulted in the net fission-product activity. To permit an eventual normalization of foil mass, each net counting rate was divided by the plutonium mass content of the monitor foil (12.875 mg). Finally, a decay curve giving the net fission-product activity per mg was plotted as a function of time.

b. Each traverse foil (of a total of 110) was counted in Band B under identical conditions of geometry, background effects were subtracted, and the resulting fission-product activity was divided by the plutonium mass content of the foil. To eliminate the effects of fission-product decay during the foil-counting operations and to normalize the effects of reactor power changes between scans, each mass-normalized fission-product counting rate was divided by a value selected from the smoothed monitor-decay curve for the specific time of counting. This procedure resulted in a set of values, one for each foil, in terms of fissions per monitor fission. Since the monitor foil was located close to the axial and radial centers of symmetry in the core, values obtained for the various foils ranged from a high of essentially unity to a low of 0.46 at the upper and outer edge of the core.

c. The number of fissions per monitor fission for a given thimble position was plotted as a function of elevation in the reactor, with the lower support plate taken as an arbitrary reference zero. In this way, a family of smooth curves, one for each thimble position, was established, with the radial distance from core center appearing parametrically.

d. Based on the number of fissions per monitor fission at discrete radial and axial positions, a second set of curves was drawn. From this set, the number of fissions per monitor fission was plotted as a function of radius, with the elevation appearing parametrically. Parametric values of elevation were chosen to coincide with the midpoint of approximate 1-in. vertical increments taken axially along a typical fuel rod. From the second set of curves, it was possible to estimate the number of fissions per monitor fission for any given fuel-rod position at each vertical increment. An actual traverse curve for the plutonium fission distribution above midplane (8.17 in.) is shown in Fig. 17. A corresponding curve for the fission distribution below midplane is shown in Fig. 18. To indicate the degree

of coverage, thimble locations (rod positions) have been designated. Figures 17 and 18 indicate that the plutonium fission distribution is relatively flat for radii less than 1 in. For radii greater than 1.5 in., the fission-rate distribution decreases sharply with increasing distance from core center. Values taken from Fig. 17 for an elevation of 8.50 in., slightly above core center, result in a value of 1.40 for the center-to-edge fission ratio.

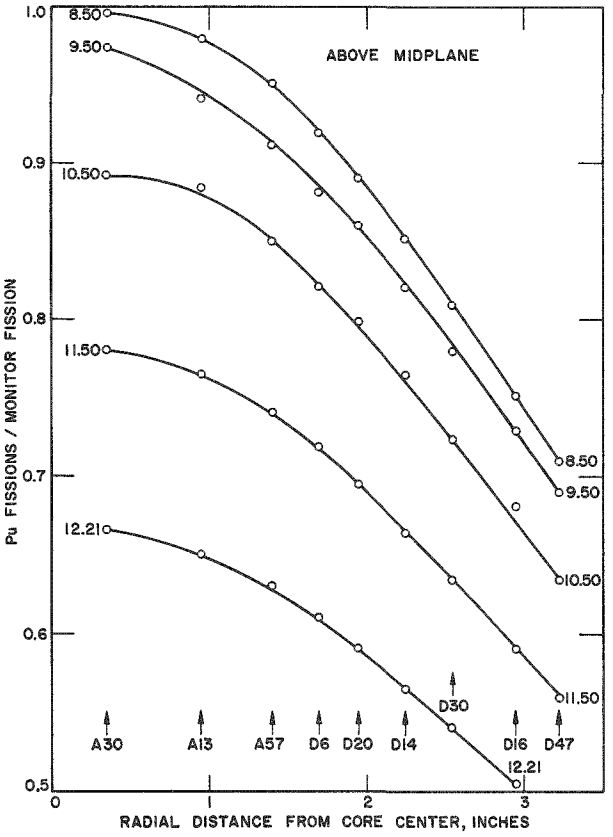

Fig. 17. Plutonium Fission Distribution in Core above Midplane

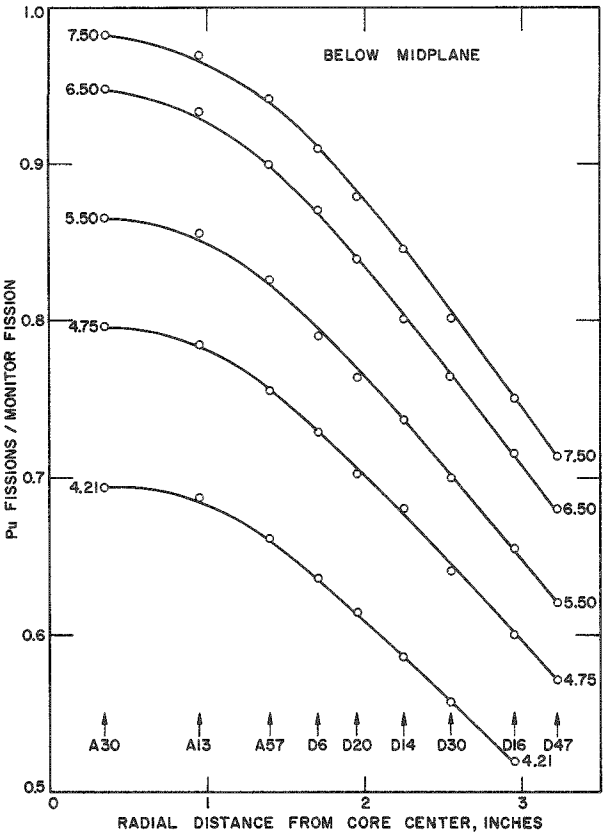

Fig. 18. Plutonium Fission Distribution in Core below Midplane

The actual integration of the fission pattern over the volume of the core is discussed in Section I; the conversion of relative-to-absolute units of fission is treated in Section J.

2. U^{235} Fission Distribution

Fission distributions for U^{235} were established in a manner analogous to the method described above for plutonium. To minimize corrections for the effects of U^{238} fission in the 93.2% enriched material, the monitor foils were irradiated at a fixed reproducible location in the graphite region. U^{235}:U^{238} fission-ratio measurements demonstrated that the effects of U^{238} fissions in the enriched foil are negligible under these conditions.

The results of enriched-foil traverse measurements in the radial and axial blankets are shown in Figs. 19 and 20. Values for elevation,

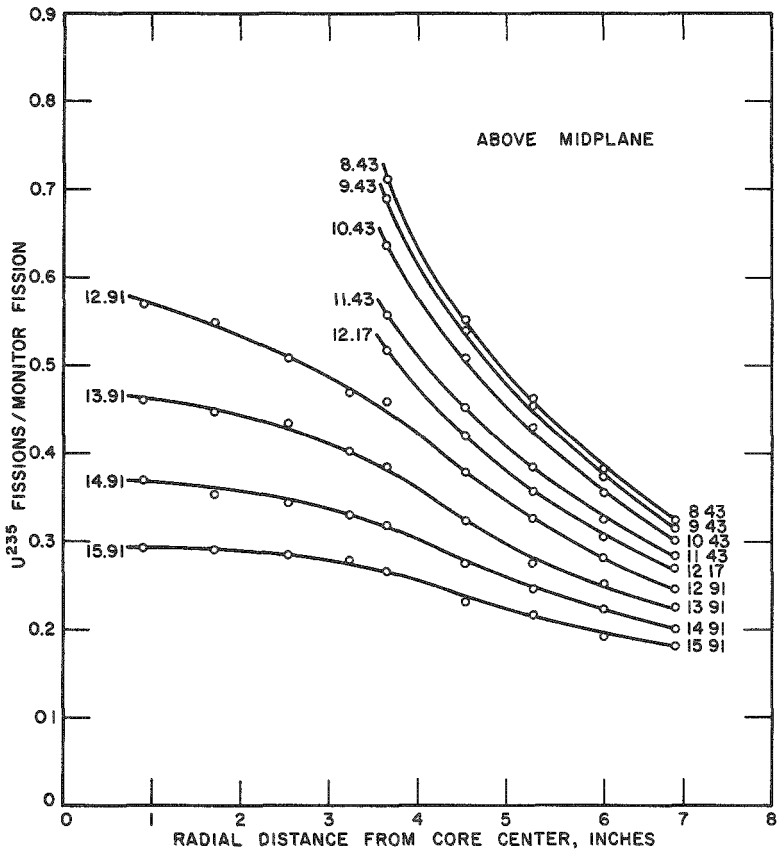

Fig. 19

U^{235} Fission Distribution in Inner Blanket above Midplane

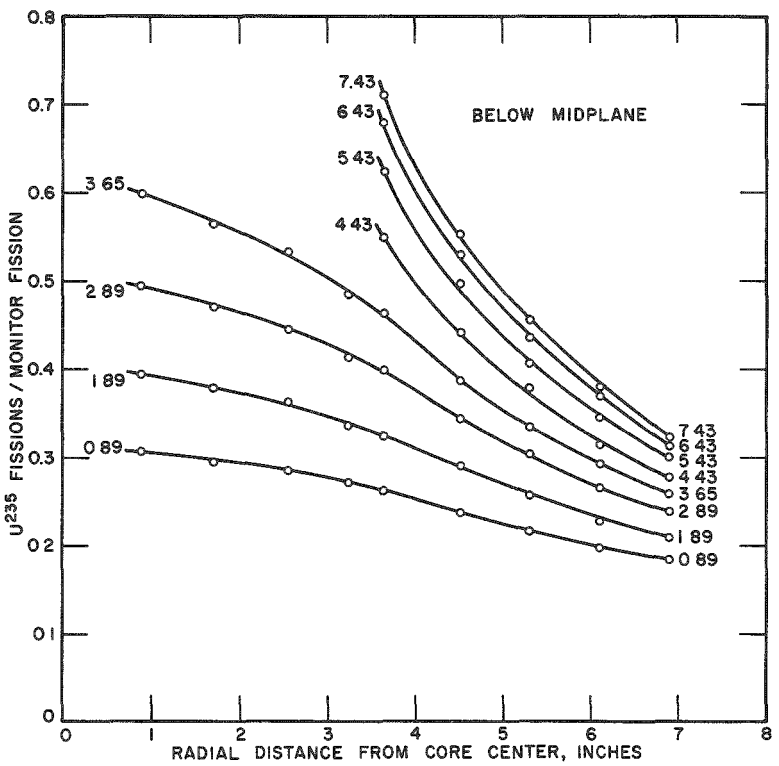

Fig. 20

U^{235} Fission Distribution in Inner Blanket below Midplane

in convenient units for subsequent mass-fission integrations, are given parametrically. Similar data for the heavy outer uranium blanket (cup) are given in Figs. 21 and 22. In this case, the arbitrary zero of elevation has been taken as the top of the shielding pedestal on which the cup rests. Ratio values are plotted as a function of radial distance from the inner edge of the cup, with values of elevation appearing parametrically.

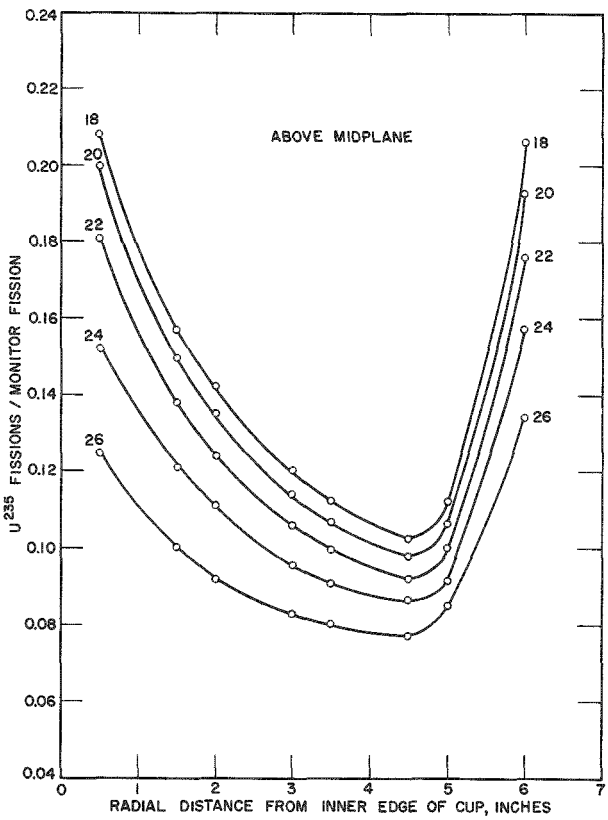

Fig. 21. U^{235} Fission Distribution in Outer Blanket above Midplane

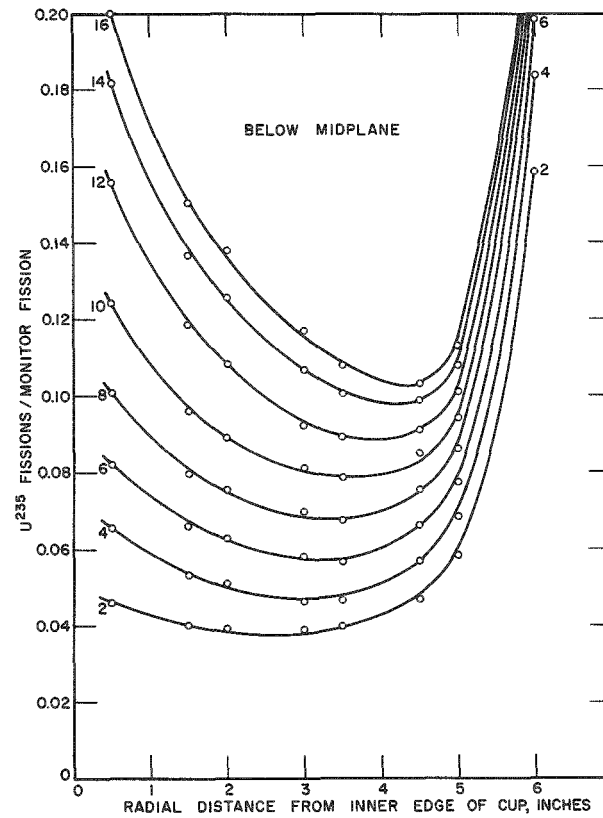

Fig. 22. U^{235} Fission Distribution in Outer Blanket below Midplane

3. U^{238} Capture Distribution

The organization of counting data for U^{238} into a form useful for the eventual evaluation of the total number of captures involved the following operations:

a. The irradiated depleted monitor foil, located at an elevation of 12.34 in. in thimble position A-30, was counted periodically (every 30 min) in both channels A and B.

b. Corrections for room and foil background, determined for each channel, were subtracted from the respective gross counting rates. This procedure resulted in two components: one (in channel A) consisted

of true Np^{239} events, plus events originating from fission-product decay; the other component (in channel B) consisted of true fission-product events. Based on the time elapsed from the end of the irradiation, a value for the ratio B:A was read from the calibration curve in Fig. 10. The fission-product component in Band A was then established from the B:A ratio and the corrected counting rate for channel B.

c. Subtraction of the Band A fission-product component from the background-corrected gross counting rate for Band A gave the true Np^{239} activity in Band A. Division of this value by the mass of the monitor foil resulted in time-dependent values for the number of capture events per gram of monitor foil. The data were plotted as a function of time, and a smooth curve was drawn through the points.

d. Between readings of the monitor-foil activity, each depleted traverse foil was counted in both Bands A and B. Corrections for room and foil background effects and for fission-product activity in Band A were applied in the manner described above. The Band A (Np^{239}) component was divided twice, first by the foil mass and then by the value obtained from the monitor decay curve for the number of capture events per gram of monitor foil. This procedure resulted in a value, for each foil, of the number of captures per monitor capture. Corrections for Np^{239} decay and for variations in reactor power between scans were eliminated by the various normalization procedures.

e. Values for the number of captures per monitor capture were then plotted as a function of elevation, with radial distance from the core center as a parameter. From the resulting family of curves, a second set of curves was plotted, this time with elevation considered parametrically and with the number of captures per monitor capture plotted as a function of radial distance from core center. The results for the inner blanket are given in Figs. 23 and 24, and for the heavy uranium cup in Figs. 25 and 26.

4. U^{238} Fission Distribution

The counting rates in Band B for the irradiated depleted foils were used indirectly to evaluate the fast-fission effect, i.e., the ratio of the number of fissions in fertile material to the number of absorptions in fissile material. Since the depleted monitor foils were located at a position of extremely hard neutron flux, at 12.34 in. elevation in A-30, a large fraction of the gross fission-product activity resulted from fast fissions in U^{238}. By means of a measured value of 7.8 for the U^{235}:U^{238} fission-product-activity ratio from auxiliary experiments in the core, the fraction of fission-product activity originating in the 0.22% abundant U^{235} isotope was shown to be only 1.6%. The effective half-life for gross fission-product decay in the depleted monitor foil, then, was virtually indistinguishable from that of pure U^{238} fission products.

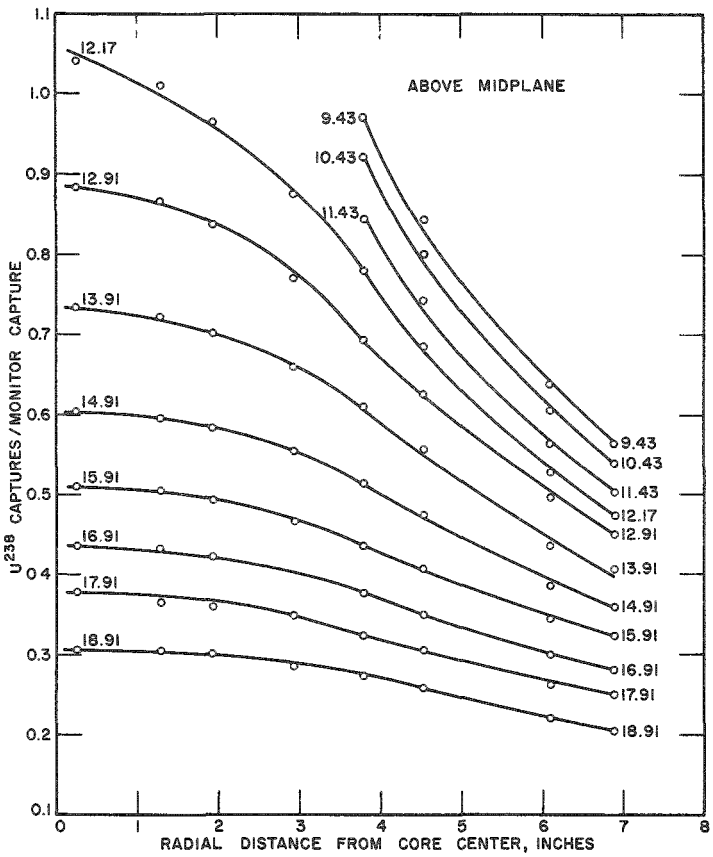

Fig. 23

U^{238} Capture Distribution in Inner Blanket above Midplane

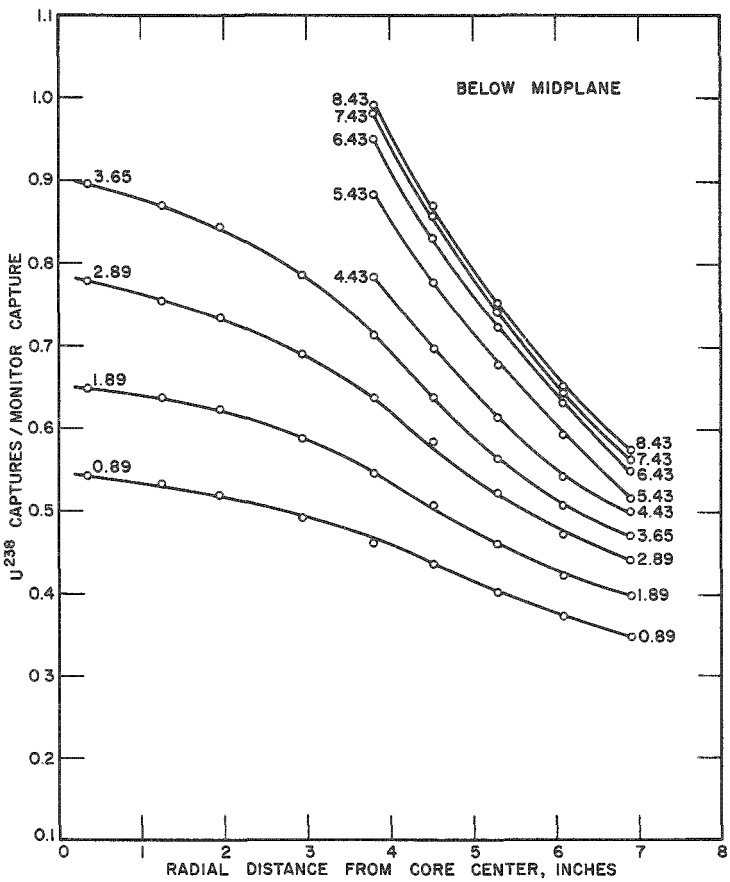

Fig. 24

U^{238} Capture Distribution in Inner Blanket below Midplane

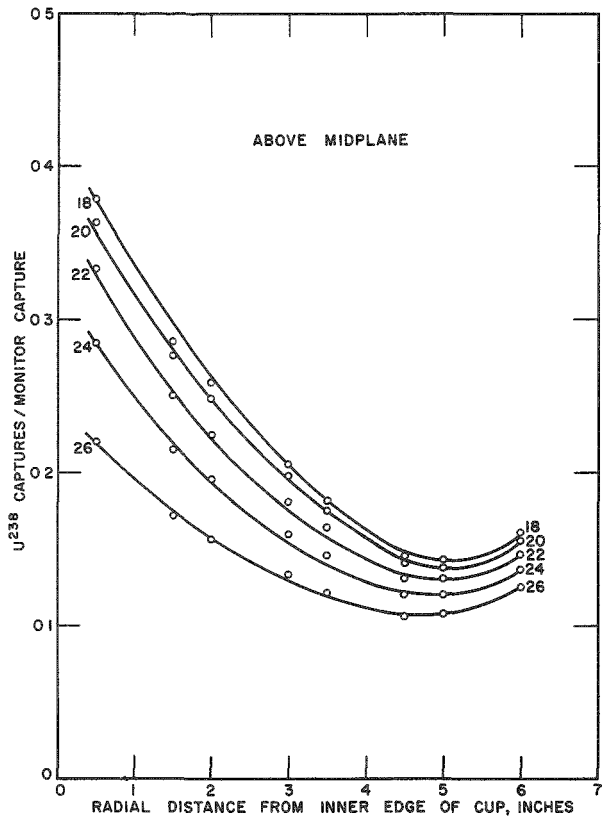

Fig. 25. U^{238} Capture Distribution in Outer Blanket above Midplane

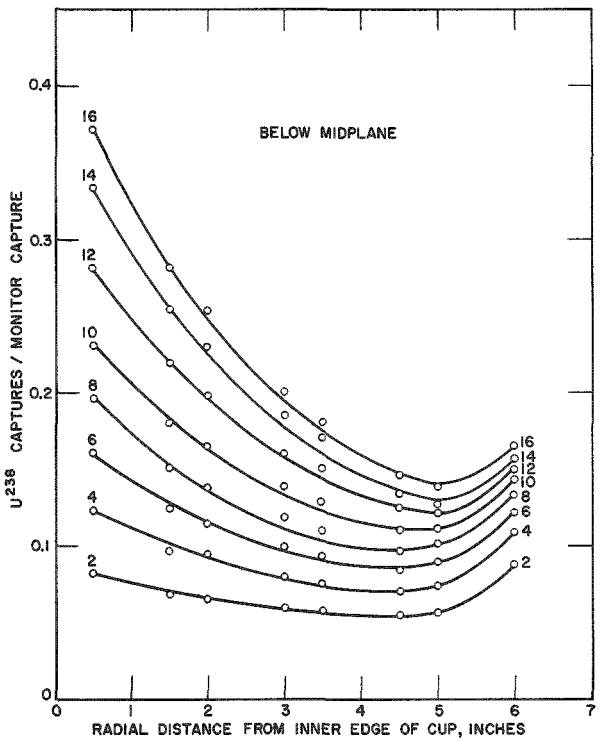

Fig. 26. U^{238} Capture Distribution in Outer Blanket below Midplane

If a tentative assumption be made that the effective half-lives of U^{235} and U^{238} fission products are indistinguishable, a simple correction for the effects of U^{235} fission products in the depleted foil may be applied. The above assumption is not, of course, completely valid, since it is known that the effective half-lives do differ significantly. However, for this evaluation, errors introduced through this assumption are relatively minor, since the region of greatest U^{238} fission activity (near the core) is also the region where the U^{235}:U^{238} fission ratio is a minimum. In outer regions of the blanket where the U^{235}:U^{238} fission ratio is large, the relative U^{238} fission effect is small.

An illustration of the magnitude of the errors involved as a result of the above assumption is instructive. If the contribution of U^{235} fission products to gross-fission-product activity is neglected for blanket material located within 4 in. of the core-blanket interface, the effect on the U^{238} fission component would be an overestimate of only 3%. For blanket material closer to the core, where the fast-fission effect is large, the corresponding error is even smaller.

As an additional argument, studies of the gross decay rate of depleted foils irradiated at core center and at the outer edges of the inner

blanket failed to reveal a significant difference in the effective half-lives for gross-fission-product decay. Because of this, and because first-order corrections for the effects of U^{235} fissions were applied, it follows that the evaluation of the fast-fission effect is acceptably accurate.

With the use of the above assumptions, the number of U^{235} fission events per gram of depleted foil is given by the following equation:

$$N_d(25) = R_{25}F_{25}P_d(25)/P_e(25), \tag{9}$$

where R_{25} is the number of U^{235} fissions per enriched monitor fission, F_{25} is the number of fissions per gram of enriched monitor foil, and $P_d(25)$ and $P_e(25)$ are the isotopic abundances of U^{235} in the depleted and enriched uranium foils, respectively. Similarly, the total number of fissions per gram of depleted foil is given by

$$N_d(28) = R_{28}F_{28}, \tag{10}$$

where R_{28} is the number of fissions per depleted monitor fission, and F_{28} is the number of fissions per gram of depleted foil. As discussed in Section IV-J, F_{25} and F_{28} were obtained through radiochemical analyses. The number of U^{238} fissions in the depleted traverse foil is closely approximated by the difference between equations (10) and (9), i.e.,

$$N'_d(28) = R_{28}F_{28} - \frac{R_{25}F_{25}P_d(25)}{P_e(25)}. \tag{11}$$

The number of fast fissions per gram of depleted material may then be found from equation (11). Care must be taken, of course, to evaluate R_{25} and R_{28} at identical radial and axial coordinates within the blanket.

In the actual integration of fast-fission events over the volume of the blanket, measured values for F_{25} and F_{28} were substituted into equation (11) (see Sections IV-I and IV-J).

A family of curves giving the number of fissions per gram of depleted material is shown in Figs. 27 and 28. Although the information given is in absolute units (rather than a ratio as given previously), a direct intercomparison of U^{235}, U^{238}, and Pu^{239} fissions is possible by the results of the radiochemical calibrations (see Section IV-J).

I. Integration of Fission and Capture Patterns

Any one of several slightly differing methods may be used to integrate the various capture and fission patterns over the volume of the system. Since each method is capable of essentially the same degree of accuracy, the actual choice was dictated by matters of simplicity. The

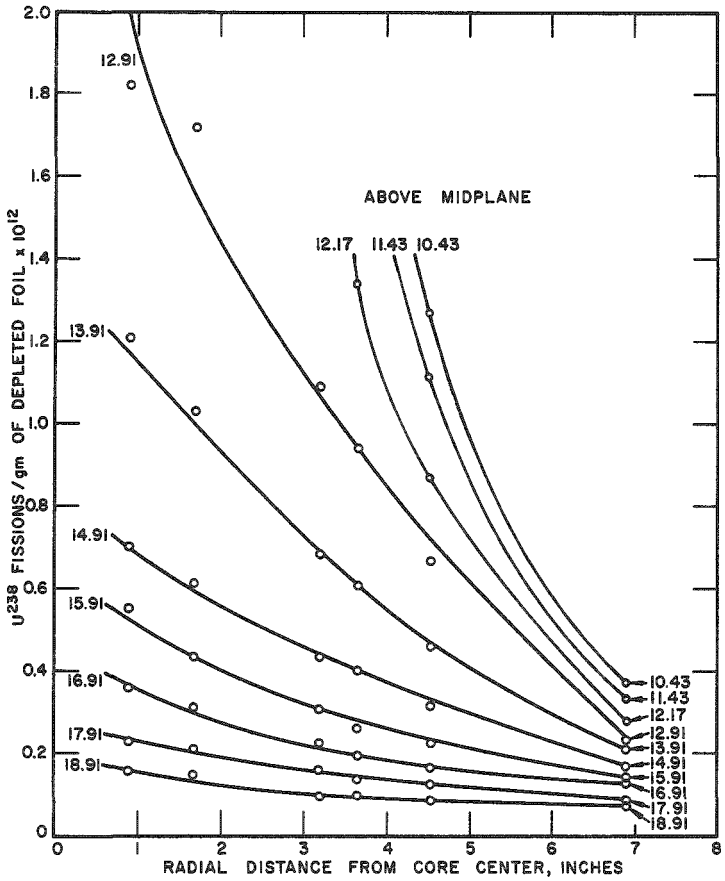

Fig. 27

U^{238} Fission Distribution in Inner Blanket above Midplane (Absolute Units)

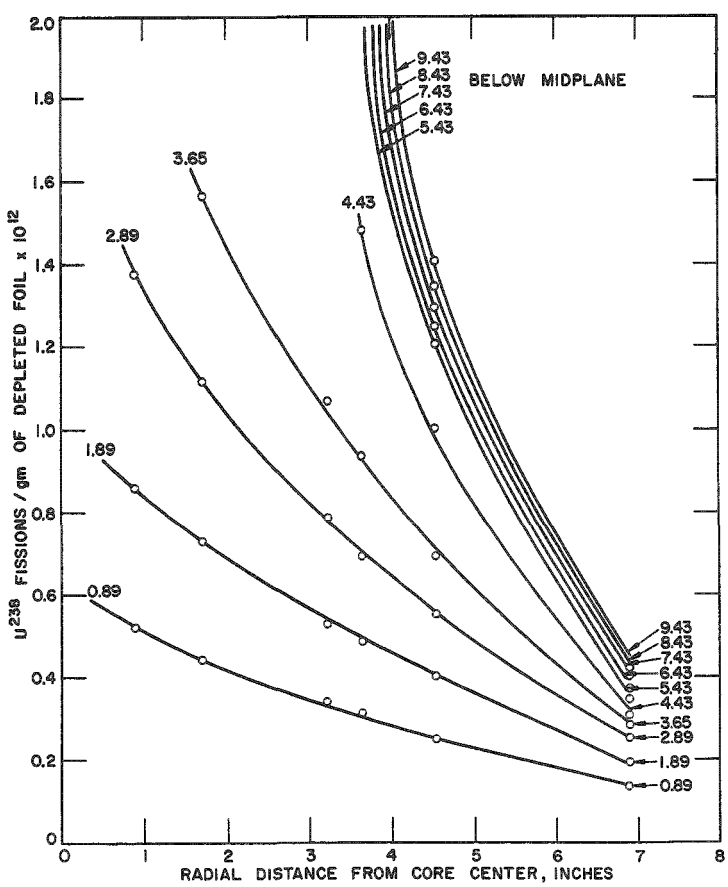

Fig. 28

U^{238} Fission Distribution in Inner Blanket below Midplane (Absolute Units)

method used consisted of evaluating the total number of events (fission or capture) for a specified fuel or blanket rod. Each value so found was multiplied by the redundancy of the rod position, i.e., by the number of rods occupying the same radial position. Information pertinent to redundancy and radial position is summarized in Table VI. A final summation over all rods in the system leads to values for the total number of fissions or captures. The actual critical mass of the cold clean reactor was measured as 327 fuel rods, or 28.714 kg Pu (all isotopes). However, the integration of fission and capture patterns was based on an adjusted loading of 320 fuel rods, since this figure is more realistic when the effects of artificial voids in the blanket and cup position are considered.(25)

Table VI

ROD POSITIONS AND REDUNDANCY

Rod Position	Distance (in.)	Redundancy	Rod Position	Distance (in.)	Redundancy	Rod Position	Distance (in.)	Redundancy
A-22	0.348	6	G-21	3.480	6	L-25	5.406	6
A-21	0.613	12	G-14	3.488	12	M-3	5.438	12
A-14	0.696	6	G-8	3.550	12	L-20	5.457	12
A-13	0.938	6	G-3	3.637	12	L-26	5.645	12
A-7	1.044	6	G-13	3.800	12	M-13	5.718	12
A-12	1.238	6	G-7	3.813	12	L-21	5.760	12
A-6	1.281	12	G-2	3.887	12	M-8	5.775	12
A-1	1.392	6	G-12	4.105	6	M-4	5.865	12
G-50	1.637	6	G-6	4.113	12	L-31	5.865	6
G-43	1.689	12	G-1	4.156	12	L-27	5.917	12
G-35	1.762	12	L-1	3.602	6	L-32	6.092	12
G-42	1.950	12	L-2	3.832	12	M-19	6.094	12
G-34	2.012	12	L-6	4.042	6	M-14	5.125	12
G-26	2.137	12	L-3	4.125	12	M-9	6.197	12
G-41	2.250	6	L-7	4.292	12	L-36	6.312	6
G-33	2.262	12	L-4	4.437	12	M-26	6.438	6
G-25	2.363	12	L-12	4.500	6	M-20	6.500	12
G-18	2.500	12	M-5	4.525	12	M-15	6.550	12
G-32	2.563	12	L-8	4.570	12	M-27	6.885	12
G-24	2.613	12	M-1	4.574	12	M-21	6.906	12
G-17	2.700	12	L-13	4.750	12			
G-11	2.844	12	L-9	4.875	12			
G-23	2.887	12	M-11	4.927	6			
G-16	2.938	12	M-6	4.938	12			
G-10	3.063	12	M-2	5.000	12			
G-22	3.175	12	L-14	5.010	12			
G-5	3.187	12	L-19	5.192	12			
G-15	3.218	12	M-12	5.313	12			
G-9	3.292	12	L-15	5.317	12			
G-4	3.395	12	M-7	5.363	12			

1. Integration of Pu^{239} Fissions and Captures

A schematic diagram of the plutonium section of a Mark-IV fuel rod is shown in Fig. 29. Plutonium fuel extends from an elevation (above the lower support plate) of 3.927 to 12.411 in., so that the total column height is 8.484 in. The column has been divided into ten vertical increments, the midpoints of which are defined in the diagram. For purposes of integration, the intensity of the fission rate was evaluated at the incremental midpoint.

The mass of each increment was established indirectly from critical mass values. With a value of 28.714 kg Pu (all isotopes) for the

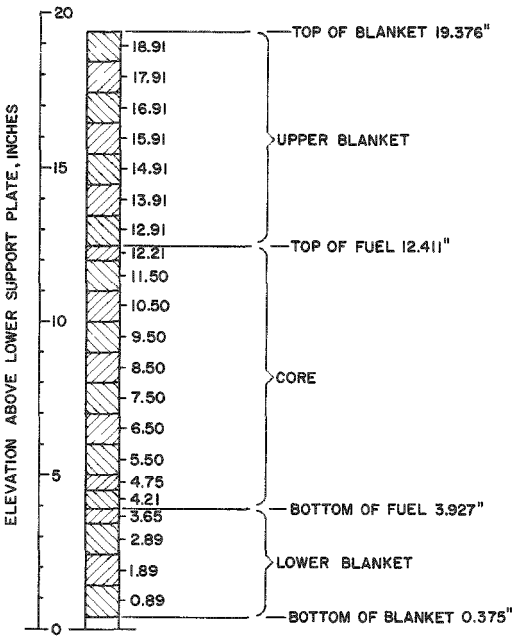

Fig. 29. Integration Increments for Mark-IV Fuel Rod

critical mass (327 fuel rods), the mass of plutonium per rod is 87.81 gm and the mass of plutonium per inch is 87.81/8.484, or 10.35 gm/in. Hence, multiplication of the fission intensity in fissions per monitor fission (from Figs. 17 and 18) by the mass of the increment, followed by a summation over the 8.484-in. column, gives the number of fissions per monitor fission for a specific rod. Multiplication by the redundancy (from Table VI) and summation over all 320 rods give the total number of fissions per monitor fission. Finally, multiplication by the number of monitor fissions per gram of monitor foil gives the total number of fissions (see Section IV-J).

Although this procedure leads to an evaluation of the total number of fissions, it fails to consider the effects of parasitic capture in Pu^{239}. Since the definition of breeding ratio specifies the total destruction of Pu^{239}, the effects of capture must be included. Although specific capture measurements were not carried out on the Mark-IV loading, use may be made of the results of measurements by Kafalas et al.,(26) who established a value of α for Pu^{239} as a function of radial distance and elevation in a U^{235}-fueled loading in EBR-I. Their results (in somewhat different form) are summarized in Fig. 30.

The application of the capture data as a correction to the Mark-IV data was manifested by multiplying the integrated Pu^{239} fission values for a particular rod group by the value of $1 + \alpha$ selected from Fig. 30. The results of the integration of both fissions and fissions-plus-captures are summarized in Table VII.

2. Integration of U^{235} Fissions and Captures

The integration of U^{235} fissions and capture patterns over

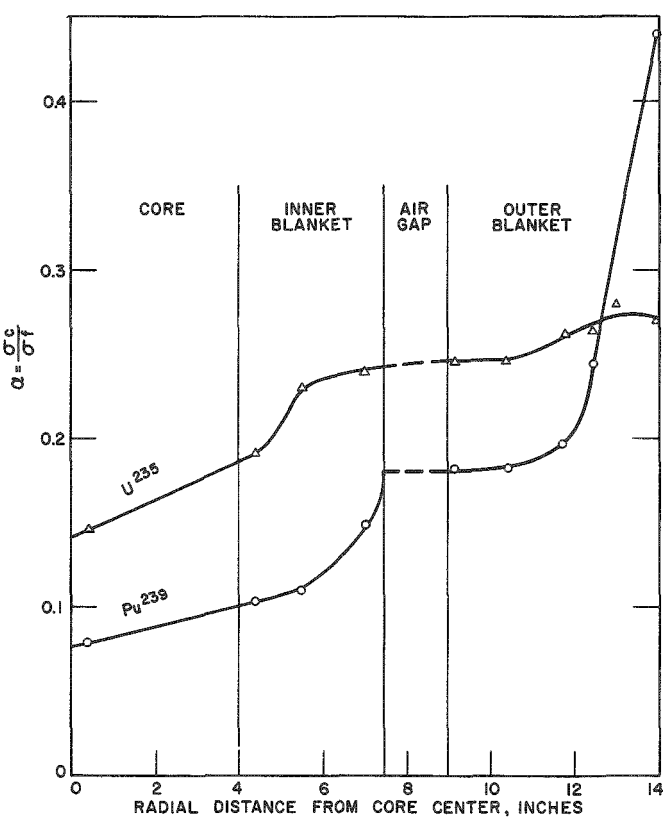

Fig. 30. Alpha for U^{235} and Pu^{239} in EBR-I (see Ref. 26)

Table VII

INTEGRATION OF PLUTONIUM FISSIONS AND CAPTURES

(1)	(2)	(3)	(4)*	(5)	(6)**
Rod Position	Number of Rods (Redundancy)	Rod Distance from Center (in.)		$1 + \alpha_{Pu^{239}}$	(4) x (5)
A-22	6	0.348	465.76	1.078	502.09
A-21	6	0.613	464.02	1.079	501.79
A-14	6	0.696	463.18	1.080	500.23
A-13	12	0.938	919.06	1.081	993.50
A-7	6	1.044	457.28	1.082	494.77
A-12	6	1.238	449.83	1.083	487.17
A-6	12	1.281	892.96	1.084	967.97
A-1	6	1.392	443.32	1.084	481.64
G-50	6	1.637	431.58	1.085	468.26
G-43	12	1.688	858.18	1.086	931.98
G-35	12	1.762	850.86	1.087	924.88
G-42	12	1.950	823.79	1.088	896.28
G-34	12	2.012	822.67	1.088	895.06
G-26	12	2.137	811.62	1.089	883.85
G-41	6	2.250	397.00	1.090	432.73
G-33	12	2.262	792.26	1.090	863.56
G-25	12	2.363	777.80	1.091	848.58
G-18	12	2.500	761.95	1.092	832.04
G-32	12	2.563	754.37	1.092	823.77
G-24	12	2.613	747.88	1.092	816.68
G-17	12	2.700	741.54	1.093	810.50
G-11	12	2.844	717.20	1.093	783.90
G-23	12	2.887	710.26	1.094	777.02
G-16	12	2.938	704.83	1.094	771.08
G-10	12	3.063	690.06	1.095	755.62
G-22	12	3.175	674.36	1.095	738.42
G-5	12	3.187	671.78	1.095	735.60
G-15	12	3.218	668.28	1.095	731.76
G-9	12	3.292	655.46	1.095	717.73
G-4	12	3.395	642.07	1.096	703.71
G-21	6	3.480	315.46	1.097	381.95
G-14	2	3.488	113.89	1.097	124.94
	320		20,680.59		22,578.76

*Column 4 is $\frac{\text{fissions x mass of plutonium (all isotopes)}}{\text{monitor fission}}$.

**Column 6 is $\frac{\text{fissions x mass of plutonium (all isotopes) x } (1 + \alpha_{Pu^{239}})}{\text{monitor fission}}$

the inner blanket was made by the general procedure outlined above. Vertical mass increments along each rod were selected, each increment was multiplied by the corresponding number of fissions per monitor fission (from Figs. 19 and 20), and the result for each rod was summed. Interpretation in terms of total fissions involved a multiplication for rod redundancy, a summation over all rod groups, and finally a conversion to absolute units (see Section IV-J).

To convert fission to capture information, the rod group fission values were multiplied by an appropriate value of $1 + \alpha$ taken from Fig. 30. Information leading to the evaluation of total fissions and captures in the inner blanket is summarized in Tables VIII, IX, and X.

Table VIII

INTEGRATION OF U^{235} FISSIONS AND CAPTURES OVER MARK-IV UPPER AND LOWER BLANKET

(1)	(2)	(3)	(4)	(5)	(6)*
Average Radius of Rod Group	Redundancy	Fissions per Monitor Fission x Mass of Blanket Material	Total (2) x (3)	$1 + \alpha_{25}$	(5) x (4)
0.348	60	52.6	3.159×10^3	1.145	3.617×10^3
1.70	30	52.4	1.573×10^3	1.160	1.824×10^3
2.00	24	51.8	1.242×10^3	1.165	1.447×10^3
2.26	42	51.3	2.153×10^3	1.167	2.512×10^3
2.60	48	50.7	2.431×10^3	1.172	2.850×10^3
2.90	36	49.4	1.779×10^3	1.173	2.087×10^3
3.15	60	48.2	2.894×10^3	1.176	3.403×10^3
3.44	20	47.3	0.945×10^3	1.180	1.115×10^3
	320		16.176×10^3		18.855×10^3

*Column 6 is the sum over a given rod group of

$$\frac{\text{fissions x mass of blanket material x } (1+\alpha_{25})}{\text{monitor fission}}$$

$$\frac{\text{fissions x grams of } U^{235}}{\text{monitor fission}} = 16.176 \times 10^3 \times 0.0022 = 35.59$$

$$\frac{\text{(captures plus fissions) x grams of } U^{235}}{\text{monitor fission}} = \frac{35.59 \times 18.855}{16.176} = 41.48$$

$$\frac{\text{captures x grams of } U^{235}}{\text{monitor fission}} = 41.48 - 35.59 = 5.89$$

Table IX

INTEGRATION OF U^{235} FISSIONS AND CAPTURES OVER MARK-IV BLANKET

(1)	(2)	(3)	(4)	(5)	(6)*
Average Radius of Rod Group	Redundancy	Fissions per Monitor Fission x Mass of Blanket Material	Total (2) x (3)	$1 + \gamma_{25}$	(5) x (4)
3.60	34	124.7	4.239×10^3	1.182	5.011×10^3
3.80	36	119.0	4.285×10^3	1.184	5.074×10^3
4.10	30	110.2	3.307×10^3	1.187	3.925×10^3
	100		11.831×10^3		14.010×10^3

*Column 6 is the sum over a given rod group of

$$\frac{\text{fissions} \times \text{mass of blanket material} \times (1 + \gamma_{25})}{\text{monitor fission}}$$

$$\frac{\text{fissions} \times \text{grams of } U^{235}}{\text{monitor fission}} = 11.831 \times 10^3 \times 0.0022 = 26.02$$

$$\frac{(\text{captures plus fissions}) \times \text{grams of } U^{235}}{\text{monitor fission}} = \frac{26.02 \times 14.010}{11.831} = 30.81$$

$$\frac{\text{captures} \times \text{grams of } U^{235}}{\text{monitor fission}} = 30.81 - 26.02 = 4.79$$

Table X

INTEGRATION OF U^{235} FISSIONS AND CAPTURES OVER MARK-III BLANKET

(1)	(2)	(3)	(4)	(5)	(6)*
Average Radius of Rod Group	Redundancy	Fissions per Monitor Fission x Mass of Blanket Material	Total (2) x (3)	$1 + \gamma_{25}$	(5) x (4)
3.70	18	270.0	4.860×10^3	1.183	5.749×10^3
4.20	30	244.5	7.334×10^3	1.188	8.713×10^3
4.50	52	230.8	12.002×10^3	1.195	14.343×10^3
4.90	42	203.7	8.554×10^3	1.206	10.316×10^3
5.10	36	195.5	7.039×10^3	1.213	8.538×10^3
5.40	66	185.3	12.232×10^3	1.225	14.983×10^3
5.80	78	173.1	13.502×10^3	1.233	16.648×10^3
6.50	110	156.0	17.158×10^3	1.238	21.241×10^3
	432		82.681×10^3		100.531×10^3

*Column 6 is the sum over a given rod group of

$$\frac{\text{fissions} \times \text{mass of blanket material} \times (1 + \gamma_{25})}{\text{monitor fission}}$$

$$\frac{\text{fissions} \times \text{grams of } U^{235}}{\text{monitor fission}} = 82.68 \times 10^3 \times 0.00715 \times 0.98 = 579.3$$

$$\frac{(\text{captures plus fissions}) \times \text{grams of } U^{235}}{\text{monitor fission}} = \frac{579.3 \times 100.53}{82.68} = 704.4$$

$$\frac{\text{captures} \times \text{grams of } U^{235}}{\text{monitor fission}} = 704.4 - 579.3 = 125.1$$

To simplify operations, the inner blanket integration was divided into three parts, namely, integrations over the upper and lower blanket sections of the Mark-IV fuel rods, over the Mark-IV blanket rods, and over the Mark-III blanket rods. The division is required mainly because the Mark-IV blanket material consists of unalloyed depleted uranium with a density of 19.0 gm/cm^3, whereas the Mark-III blanket material consists of a 2% Zr-natural uranium alloy with a density of 17.95 gm/cm^3.

The integration of U^{235} fission-and-capture data for the massive natural uranium outer blanket (cup) was complicated by the physical irregularity of the cup and by the unusual fission distribution. The division of a single brick (all 84 bricks are identical) into workable increments is illustrated in Fig. 31. Six irregularly shaped sections (labeled A through F in Fig. 31) were selected. The effect of the uranium control rods was considered by arbitrarily assigning half of the associated volume to each of the increments, A and B. Pertinent volume and mass information, based on a natural uranium metal density of 19.0 gm/cm^3, is summarized in Table XI.

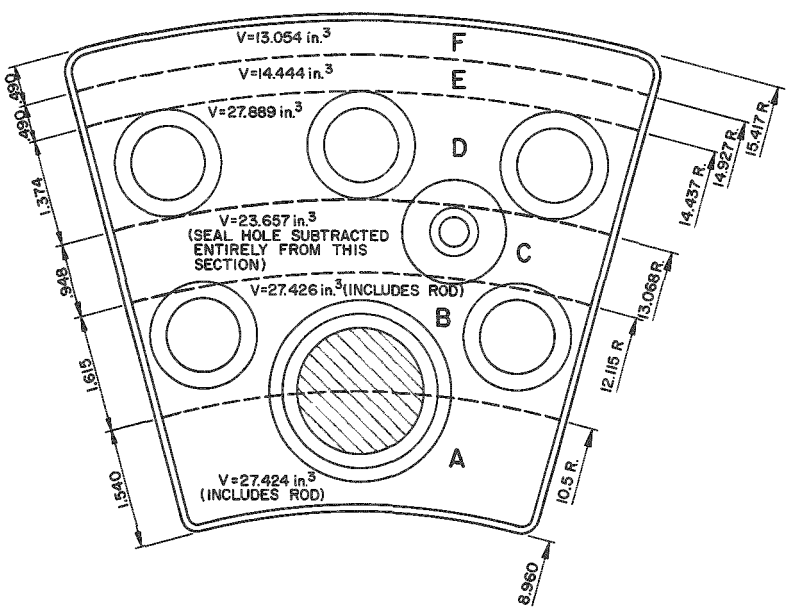

Fig. 31

Integration Increments for Uranium Cup

Table XI

INTEGRATION INCREMENTS FOR URANIUM CUP

Increment	Volume (cm^3)	Mass (gm)	Mass of Column (kg)	Mass of Column (gm/in.)
A	453.6	8618	60.33	2224
B	453.6	8618	60.33	2224
C	391.3	7435	52.05	1919
D	461.3	8765	61.36	2262
E	238.9	4539	31.77	1171
F	215.9	4102	28.71	1059

From Figs. 21 and 22, which give the U^{235} fission profile as a function of radius, it is clear that an intensity value selected at a radius midway between the inner and outer limits of the radial increment will not be a true average value. Accordingly, it was necessary to determine the centroidal value of the fission intensity for each radial increment. As an additional complication, centroidal values of intensity had to be determined as a function of elevation. The procedure used is based on the following considerations. Each increment was divided into eight cylindrical subincrements. The integrated value for the complete increment is then approximated by the following expression:

$$a_1 dV_1 + a_2 dV_2 + \ldots + a_8 dV_8 = \bar{a} V, \tag{12}$$

where the a's are the average intensities of each of the cylindrical subincrements for a given elevation, the dV_i's are the volumes of the respective cylindrical increments, V is the total volume, and $\bar{a}$ is the centroidal value of fission intensity. Hence,

$$\bar{a} = \frac{a_1 dV_1 + a_2 dV_2 + \ldots + a_8 dV_8}{V}. \tag{13}$$

Since

$$\Delta(V_i)_h = 2\pi r_i h \Delta r_i, \tag{14}$$

$\bar{a}$ can be evaluated as a function of elevation h. To simplify the many evaluations, $\bar{a}$ was established for each radial increment (i.e., A through F) at elevations of 2, 10, and 17 in. At each of these elevations, the radius at which the experimentally measured value for intensity coincided with $\bar{a}$ was noted, and a straight line was drawn through the points. Thus, intensity values representative of the volume increment for each radial and vertical increment were established. Multiplication of the intensity value by the mass of the increment, followed by summing over all increments and over all bricks, permitted an eventual determination of total U^{235} fissions in the cup. The conversion of relative numbers to absolute fissions is given in Section IV-J. Fission events were converted to total events in the manner previously described, by use of the data of Fig. 30 for α_{25}. Information pertinent to an evaluation of total U^{235} fissions and captures in the cup is summarized in Table XII. Fission and capture information for all blanket regions is summarized in Table XIII.

3. Integration of U^{238} Captures

The integration of Np^{239} activity over the volume of the inner and outer blankets was carried out in a similar manner. For simplicity, the integration was conducted over the volume increments used for the integration of U^{235} fissions and captures. The results for the various blanket regions are summarized in Table XIV.

Table XII

INTEGRATION OF U^{235} FISSIONS AND CAPTURES OVER THE OUTER BLANKET (CUP)

(One vertical column of seven bricks)

(1)	(2)	(3)	(4)
Increment	Fissions per Monitor Fission x Mass of Blanket Material	$1 + \alpha_{25}$	(2) x (3)
A	7,472	1.245	9,302
B	5,550	1.255	6,965
C	4,179	1.270	5,307
D	5,156	1.275	6,574
E	4,753	1.270	6,036
F	6,056	1.270	7,691
	33,166		41,875

$$\frac{\text{fissions x grams of } U^{235}}{\text{monitor fission}} = 33.17 \times 10^3 \times 0.00715 \times 12 \text{ columns} = 2846$$

$$\frac{\text{(captures plus fissions) x grams of } U^{235}}{\text{monitor fission}} = \frac{2846 \times 41.88}{33.17} = 3593$$

$$\frac{\text{captures x grams of } U^{235}}{\text{monitor fission}} = 3593 - 2846 = 747$$

Table XIII

SUMMARY OF U^{235} CAPTURES AND FISSIONS OVER ALL BLANKETS

(1)	(2)*	(3)**	(4)†
Blanket Region	Fissions	Captures Plus Fissions	Captures
Upper and Lower Blankets, Mark IV	35.59	41.48	5.89
Mark-IV Blanket	26.02	30.81	4.79
Mark-III Blanket	579.3	704.4	125.1
Outer Blanket (Cup)	2,846.	3,593.	747.
	3,487.	4,370.	882.

*Column 2 is $\frac{\text{fissions x grams of } U^{235}}{\text{monitor fission}}$

**Column 3 is $\frac{\text{(captures plus fissions) x grams of } U^{235}}{\text{monitor fission}}$

†Column 4 is $\frac{\text{captures x grams of } U^{235}}{\text{monitor fission}}$

Table XIV

INTEGRATION OF U^{238} CAPTURES IN THE VARIOUS BLANKETS

Region	Captures per Monitor Capture x Grams of Blanket Material (x 10^{-4})	Grams of U^{238} per Gram of Blanket Material	Captures per Monitor Capture x Grams of U^{238} (x 10^{-4})
Mark-IV Upper and Lower Blankets	2.494	0.9978	2.489
Mark-IV Blanket	1.741	0.9978	1.737
Mark-III Blanket	13.45	0.9730*	13.09
Outer Blanket (Cup)	54.43	0.99285	54.04
Plug**	3.48	0.99285	3.46
			74.81

*Correction for 2 w/o Zr included.

**Traverses not carried out in plug. Estimate based on work of Levenson et al.[13]

4. Integration of U^{238} Fissions

The integration of U^{238} fast-fission patterns over the inner blanket involved essentially the same methods as those described above, with the exception that the integration in this case resulted directly in the total number of fast fissions. As explained in Section IV-H-4, corrections for the effects of U^{235} fission products at each volume increment were required. Accordingly, it was simpler to interpret the U^{238} fission intensity in absolute rather than relative units. The results obtained over the inner blanket are summarized in Table XV.

Table XV

SUMMARY OF U^{238} FISSION INTEGRATIONS

Region	Fissions in Blanket Material (x 10^{-16})	Grams of U^{238} per Gram of Blanket Material	Fissions in U^{238} Content of Blanket (x 10^{-16})
Mark-IV Upper and Lower Blankets	2.95	0.9978	2.94
Mark-IV Blanket	3.02	0.9978	3.01
Mark-III Blanket	14.63	0.9730*	14.23
Outer Blanket (Cup)	4.92	0.99285	4.88
			25.06

*Correction for 2 w/o Zr included.

J. Conversion of Relative Units to Absolute

With the exception of the U^{238} fast-fission integration, all results given previously have been expressed in terms of an intensity relative to that of a monitor foil multiplied by the mass of the material. Such results, by themselves, are meaningless. To compare all results on an equal power-irradiation time basis and to interpret each of the results in absolute units, a complete set of monitor foils which had been irradiated simultaneously at their respective locations were analyzed radiochemically. With

each foil (one depleted, one enriched, and one aluminum-clad plutonium) at its proper monitoring position, the reactor was operated at a power level of 10 kW for one hour. The simultaneous irradiation of all monitor foils eliminated the necessity for time and flux corrections.

Analyses for total fissions in the plutonium monitor foil were carried out by the ICPP analytical group of Phillips Petroleum Company.[27] Analyses for total fissions and captures in the depleted foil, and for total fissions in the enriched foil, were carried out by ANL personnel at the Argonne, Illinois, site.[28] The results of these analyses are summarized in Table XVI.

Table XVI

RADIOCHEMICAL ANALYSES OF MONITOR FOILS

	Enriched Foil	Depleted Foil	Plutonium Foil
Fissions	3.82×10^{13} fissions per gram of foil	3.05×10^{12} fissions per gram of foil	4.584×10^{13} fissions per gram of Pu (all isotopes)
Captures		1.99×10^{12} captures per gram of foil	

The fission results in Table XVI are based on the following yields of Mo^{99}: U^{235}, 6.1%; U^{238}, 6.3%; and Pu^{239}, 5.89%.[29] To convert the results of the various fission and capture integrations into absolute units from the data of Table XVI, corrections must be applied for the effects of other isotopes in the monitor foils.

Corrections for the effects of the U^{235} content of the depleted foil on the number of fissions per gram were applied in the following manner: a value of 7.8 for the U^{235}:U^{238} fission ratio (at the monitoring point) and an isotopic weight percent value of 99.78% for U^{238} were used. The number of fissions per gram of U^{238} in the depleted monitor foil was then found to be 3.00×10^{12}.

Since the irradiation of the enriched monitor foil was carried out in the graphite region, essentially all of the fission-product activity is the result of U^{235} fissions. Accordingly, the only correction necessary is a mass consideration which involves the abundance (6.8%) of the U^{238} isotope.

Corrections for the effects of higher plutonium isotopes in the plutonium monitor foil were hindered by the following factors: (1) a difference in isotopic content of the plutonium in fuel and in monitor foil; (2) lack of information regarding spectrum and cross-section values. For example, the isotopic composition of the fuel material averages out to the following values (in w/o): Pu^{239}, 94.4; Pu^{240}, 5.1; and Pu^{241}, 0.5. The isotopic composition of the plutonium in the monitor foil, on the other hand, is given by

the following: Pu^{239}, 94.91; Pu^{240}, 4.60; and Pu^{241}, 0.48. To allow for the relative effects of each of these species, effective cross-section values were estimated from cross-section sets given in Yiftah et al.,[30] which in turn were weighted for an EBR-I type spectrum.[31] Fission values obtained in this manner amounted to the following: Pu^{239}, 1.81 b; Pu^{240}, 0.950 b; and Pu^{241}, 2.00 b. Assume, as a first-order approximation, that the fission yields and effective fission product half-lives are the same for fissions in Pu^{239}, Pu^{240}, and Pu^{241}. The fraction of fissions originating in each of the plutonium isotopes may then be estimated from the following considerations: If x, y, and z give the number of fissions per gram for Pu^{239}, Pu^{240}, and Pu^{241}, respectively, then

$$I_{239}x + I_{240}y + I_{241}z = 4.584 \times 10^{13}, \tag{15}$$

where the I's are the isotopic abundances for the respective isotopes, and the value 4.584×10^{13} is the number of fissions per gram of plutonium (all isotopes) from radiochemical analyses. Since $x/y = 1.905$ and x/z 0.905 (from the effective fission cross sections), each term in equation (15) may be evaluated. The results are summarized in Table XVII.

Table XVII

SPECIFIC FISSION RATES OF PLUTONIUM ISOTOPES

	Pu^{239}	Pu^{240}	Pu^{241}
Fissions per gram	4.685×10^{13}	2.459×10^{13}	5.177×10^{13}
Fraction of Total Fissions in Fuel Pin	0.967×10^{13}	0.0274×10^{13}	0.0057×10^{13}

1. Pu^{239} Fissions

The number of Pu^{239} fissions may be found from the integrated fission-mass values given in Table VII and from the specific fission values of Table XVII. Hence, the number of Pu^{239} fissions in the core is

$$N_{239}^{f} = abc, \tag{16}$$

where

$$a = \frac{\text{fissions x mass of plutonium (all isotopes)}}{\text{monitor fission}};$$

$$b = \frac{Pu^{239} \text{ monitor fissions}}{\text{gram of } Pu^{239}}.$$

and

c = isotopic abundance of Pu^{239} in the fuel.

Substitution of values into equation (16) gives

$$N_{239}^{f} = (2.068 \times 10^{4})(4.685 \times 10^{13})0.944 = 0.9146 \times 10^{18} \text{ fissions.}$$

2. Pu^{239} Captures

The number of Pu^{239} captures plus fissions is given by

$$N_{239}^{f+c} = abc, \tag{17}$$

where

$$a = \frac{\text{(fissions plus captures) x mass of Pu (all isotopes)}}{\text{monitor fission}},$$

$$b = \frac{Pu^{239} \text{ monitor fissions}}{\text{gram of } Pu^{239}},$$

and

c = isotopic abundance of Pu^{239} in the fuel.

Hence,

$$N_{239}^{f+c} = (2.258 \times 10^{4})(4.685 \times 10^{13})0.944$$

$$= 0.9987 \times 10^{18} \text{ captures plus fissions.}$$

The number of captures, then, is simply the difference between equations (17) and (16), or 0.0841×10^{18}.

3. Pu^{240} Fissions

The number of Pu^{240} fissions is given by

$$N_{240}^{f} = abc, \tag{18}$$

where

$$a = \frac{\text{fissions x mass of Pu (all isotopes)}}{\text{monitor fission}},$$

$$b = \frac{Pu^{240} \text{ monitor fissions}}{\text{gram of } Pu^{240}},$$

and

c = isotopic abundance of Pu^{240} in the fuel.

Hence,

$$N^f_{240} = (2.068 \times 10^4)(2.459 \times 10^{13})0.051 = 0.0259 \times 10^{18} \text{ fissions.}$$

4. Pu^{240} Captures

The number of captures in Pu^{240} may be estimated from the relative fission and capture cross-section values, weighted for an EBR-I type spectrum.[30,31] If a fission cross section of 0.950 b and a capture cross section of 0.20 b are used, the number of captures is calculated to be

$$N^c_{240} = \frac{0.20 \times 0.0259 \times 10^{18}}{0.950} = 0.0055 \times 10^{18} \text{ captures.}$$

5. Pu^{241} Fissions

The number of Pu^{241} fissions in the core is

$$N^f_{241} = abc, \tag{19}$$

where

$$a = \frac{\text{fissions x mass of plutonium (all isotopes)}}{\text{monitor fission}},$$

$$b = \frac{Pu^{241} \text{ monitor fissions}}{\text{gram of } Pu^{241}},$$

and

c = isotopic abundance of Pu^{241} in the fuel.

Hence,

$$N^f_{241} = (2.068 \times 10^4)(5.177 \times 10^{13})0.005 = 0.0054 \times 10^{18} \text{ fissions.}$$

6. Pu^{241} Captures

If a value of α for Pu^{241} comparable to that of Pu^{239} (i.e., approximately 0.1) is assumed, the number of Pu^{241} captures is estimated to be 0.0005×10^{18}.

7. U^{235} Fissions

The number of U^{235} fissions integrated over all blankets may be found from:

$$N_{235}^{f} = ab, \tag{20}$$

where

$$a = \frac{\text{fissions x grams of } U^{235}}{\text{monitor fission}},$$

and

$$b = \frac{U^{235} \text{ monitor fissions}}{\text{gram of } U^{235}}.$$

Hence,

$$N_{235}^{f} = \frac{3487(3.82 \times 10^{13})}{0.932} = 0.1429 \times 10^{18} \text{ fissions.}$$

8. U^{235} Captures

The number of fissions plus captures integrated over all blankets is given by

$$N_{235}^{f+c} = ab, \tag{21}$$

where

$$a = \frac{(\text{fissions plus captures}) \text{ x grams of } U^{235}}{\text{monitor fission}},$$

and

$$b = \frac{U^{235} \text{ monitor fissions}}{\text{gram of } U^{235}}.$$

Hence,

$$N_{235}^{f+c} = \frac{4370(3.82 \times 10^{13})}{0.932} = 0.1791 \times 10^{18} \text{ captures plus fissions.}$$

The number of captures, then, is given by the difference between equations (21) and (20):

$$N_{235}^{c} = (0.1791 - 0.1429)10^{18} = 0.0362 \times 10^{18} \text{ captures.}$$

9. U^{238} Fissions

The number of U^{238} fissions integrated over all blankets is given in Table XV as 0.251×10^{18}.

10. U^{238} Captures

The number of U^{238} captures is given by

$$N_{238}^{c} = ab, \tag{22}$$

where

$$a = \frac{\text{captures x grams of } U^{238}}{\text{monitor capture}},$$

and

$$b = \frac{U^{238} \text{ monitor captures}}{\text{gram of } U^{238}}.$$

Hence,

$$N_{238}^{c} = \frac{(74.81 \times 10^{4})(1.99 \times 10^{12})}{0.9978} = 1.492 \times 10^{18} \text{ captures}. \tag{23}$$

11. Summary of Fissions and Captures

A summary of all fissions and captures is given in Table XVIII.

Table XVIII

SUMMARY OF FISSIONS AND CAPTURES

	Fissions ($\times 10^{-18}$)	Captures ($\times 10^{-18}$)
U^{235}	0.1429	0.0362
Pu^{239}	0.9146	0.0841
Pu^{240}	0.0259	0.0055
Pu^{241}	0.0054	0.0005
U^{238}	0.251	1.492

V. RESULTS

A. Breeding Ratio

The definition of breeding ratio given by equation (1) may be rewritten as

$$\text{B.R.} = \frac{\text{Production of } Pu^{239} \text{ and } Pu^{241}}{\text{Destruction of } U^{235}, Pu^{239}, \text{ and } Pu^{241}}, \tag{24}$$

where the destruction term in the denominator includes the effects of parasitic capture. Substitution of values from Table XVIII into equation (24) gives

$$\text{B.R.} = \frac{1.492 + 0.0055}{(0.1429 + 0.0362) + (0.9146 + 0.0841) + (0.0054 + 0.0005)} \tag{25}$$

or

$$\text{B.R.} = \frac{1.4975}{1.1837} = 1.27 \pm 0.08, \tag{26}$$

where the precision limits have been established in a manner outlined in Appendix C. From these results it follows that for every 100 atoms of fissionable material consumed, approximately 127 atoms of Pu^{239} are generated in the various breeding blankets. A relatively insignificant amount of Pu^{241} is generated in the Pu^{240} content of the core.

B. Fast-fission Bonus

If the fast-fission bonus (F.F.B.) is defined as the ratio of the number of fissions in fertile material to the number of absorptions in fissionable material:

$$\text{F.F.B.} = \frac{\text{Fissions in } U^{238} \text{ and } Pu^{240}}{\text{Fissions plus captures in } U^{235}, Pu^{239}, \text{ and } Pu^{241}}. \tag{27}$$

An evaluation may be carried out from the information of Table XVIII. Substitution of values from Table XVIII into equation (27) results in

$$\text{F.F.B.} = \frac{0.251 + 0.0259}{(0.1429 + 0.0362) + (0.9146 + 0.0841) + (0.0054 + 0.0005)} \tag{28}$$

$$= \frac{0.2769}{1.1837} = 0.23 \tag{29}$$

It follows, then, that for every 100 atoms of fuel destroyed, approximately 21 atoms of U^{238} and two atoms of Pu^{240} are fissioned.

C. Structural Absorption and Leakage

The efficiency of breeding in the EBR-I system may be estimated by considering the basic neutron-balance equation given by

$$B.G. = \frac{X_1(\nu_1-1-\alpha_1) + X_2(\nu_2-1-\alpha_2) + X_3(\nu_3-1-\alpha_3) + F_4(\nu_4-1) + F_5(\nu_5-1) - (A+L)}{X_1(1+\alpha_1) + X_2(1+\alpha_2) + X_3(1+\alpha_3)}, \quad (30)$$

where X_1, X_2, and X_3 are the fission fractions for U^{235}, Pu^{239}, and Pu^{241}, respectively, and F_4 and F_5 are the respective fission fractions for U^{238} and Pu^{240}. The subscripts 1 through 5 refer, respectively, to U^{235}, Pu^{239}, Pu^{241}, U^{238}, and Pu^{240}. The number of neutrons "wasted" (i.e., unavailable for capture in U^{238} and Pu^{240}) is given by (A+L), where A is the number of neutrons lost through capture in structural materials and coolant per fission, and L is the number of neutrons per fission leaking from the system Hence, substitution of the experimental value of 1.27 for the breeding ratio into equation (30), along with appropriate values for ν and α, permits an evaluation of the combined absorption-leakage term, (A+L)

Information from Table XVIII may be used to evaluate X_1, X_2, X_3, F_4, and F_5. Estimates of ν_1 through ν_5, based on information compiled by Okrent,[32] consist of the following: ν_1 (U^{235}), 2.50, ν_2 (Pu^{239}), 2 90, ν_3 (Pu^{241}), 2.99, ν_4 (U^{238}), 2 51; and ν_5 (Pu^{240}), 2.77. Approximate values, namely, 0 09 and 0 25, based on the work of Kafalas et al.,[26] were assumed for the ratio of capture to fission in Pu^{239} and U^{235}, respectively. Since information was not available for capture in Pu^{241}, a value of 0.10 for α_3 was arbitrarily assumed. Substitution of the various values into equation (30) results in a value of 0 66 for the combined absorption-leakage term, (A+L)

Assuming that leakage and structural absorption effects are the same for all neutrons, irrespective of their origins, the above elevation is significant in that approximately 0.66 neutron per weighted fissile absorption disappears through absorption processes in the structure and coolant as well as through leakage from the breeding blankets.

In earlier conversion-ratio measurements on a U^{235}-fueled system, Kato[15] estimated a combined absorption-leakage value of 0 44. The difference between the earlier value and the value given above may be explained, in part, on the basis of strong differences in blanket volume fractions. In earlier loadings (i.e., Mark I and II), the uranium composition of the outer radial blanket was 71 v/o. In the change from the Mark-II to the Mark-III loading (hence, Mark IV), the uranium composition was reduced to 50 v/o. The change also caused an increase in values for the volume fractions of structural materials and coolant. For example, in the Mark-II outer radial blanket the following volume percentages applied.

stainless steel, 9%; NaK, 20%. In Mark IV, however, the corresponding volume percentages are: stainless steel, 7.3%; zirconium, 18.2%; NaK, 25.6%. A further significant difference is to be found in the composition of the region included between the inner radial blanket and the uranium cup. In Mark II, the composition (in v/o) of this region was as follows: stainless steel, 23.5%; aluminum, 7.7%; Inconel, 4.1%; NaK, 30.0%. In Mark IV, on the other hand, the composition is: stainless steel, 54.1%; aluminum, 5.44%; Inconel, 2.84%; NaK, 13%. From these considerations, it seems likely that the absorption and leakage terms (i.e., A and L) are larger for the Mark-IV system, and that the difference between the values of 0.44 and 0.66 is real.

VI. DISCUSSION AND CONCLUSIONS

The value of 1.27 ± 0.08, measured for the breeding ratio of the Mark-IV loading, demonstrates the importance of Pu^{239} as a fast reactor fuel, since earlier measurements of the conversion ratio of essentially the same system fueled with U^{235} gave values of the order of unity.[13-15] The marked increase is directly attributable to a much higher value of ν for Pu^{239} and a much lower value of α. The effect on neutron economy of fissions in U^{235} is significant, since approximately 14 percent of the fissions in fissionable material occur in U^{235}.

The results also indicate the beneficial aspects of threshold fission in U^{238} and Pu^{240}. For every 100 neutrons absorbed in fuel species, approximately 21 atoms of U^{238} are fissioned. Although the Pu^{240} content of the loading is low, two atoms of Pu^{240} are also fissioned. Because of its lower threshold fission energy and a somewhat higher cross-section value, Pu^{240} is more valuable as fertile material than U^{238}.

The experimental nature of the EBR-I system is reflected by an inefficient utilization of neutrons. An estimate based on the neutron-balance equation reveals that for every absorption in fissile material approximately 0.66 neutron is "wasted," either through leakage from the assembly or through nonproductive capture in the coolant or structural materials. Clearly, the incorporation of thicker and denser breeding blankets would be reflected by a significant increase in the breeding ratio and an important reduction in the doubling time.

Finally, the results provide tangible proof that a reactor fueled with Pu^{239} can produce useful power and regenerate substantially more fuel than is consumed.

VII. ACKNOWLEDGMENTS

The authors gratefully acknowledge the assistance of Messrs. F. D. McGinnis, C. B. Doe, and other personnel of the EBR-I operating crew. The authors appreciate the cooperation of Messrs. J. Rein, W. Maeck, and D. Olson of Phillips Petroleum Company, who carried out the necessary fission-product analyses on the plutonium monitor foils. Similarly, the efforts of Mr. Roland Armani and Miss Frances Lyon of the Argonne Reactor Engineering Division are gratefully acknowledged.

APPENDIX A

Procedure for Neptunium

1. Dissolve the uranium sample in 6M HCl and enough H_2O_2 to oxidize all the uranium.(1)* Add the Np^{237} tracer,(2) and evaporate to dryness. Take up residue in enough 4M HCl to keep the uranium concentration below 5%

2. Add to this solution, per ml of solution, one drop of lanthanum carrier (5 mg La/ml), one drop of strontium carrier (10 mg Sr/ml), and one drop of 10% $KMnO_4$ solution. Agitate the solution, and allow it to stand for 10 min. Then reduce the solution by bubbling SO_2 through it for one min (the permanganate color disappears). Allow the solution to stand for 15 min.

3. Add a pinch of solid $NH_2OH \cdot HCl$, and agitate. Calculate the HCl concentration, and adjust (if necessary) to 3 to 4M. Make the solution 2.5M in HF (1.8 drops/ml), and allow 30 min for the fluoride precipitate to form.

4. Centrifuge the solution and remove the supernate. Wash the precipitate twice with 5-ml volumes of 2M HF-2M HNO_3 solution. Remove the washes with a pipette after centrifuging and add them to the supernate, which is saved for uranium recovery.

5. Add one ml of saturated H_3BO_3 solution to the precipitate, agitate, and allow to stand for 10 min. Add 2 ml conc HNO_3 with stirring, and dilute with 8 ml H_2O. Add one drop of 10% $KMnO_4$ solution, per ml of solution, and allow it to stand for 15 min.

6. Make a solution 2.5M in HF. Allow 10 min for the precipitate to form and centrifuge. Wash the precipitate twice with 2-ml portions of 2M HF-2M HNO_3 solution. Centrifuge, and add washes to the supernate from the discarded precipitate.

7. Reduce the supernate with 35% solution of $NH_2OH \cdot HCl$ until the permanganate color disappears, and add six to eight drops of the excess. Add one drop of zirconium carrier (10 mg Zr/ml) for every 2 ml of solution, agitate, and allow to stand 15 min. Add one drop of lanthanum carrier for every 2 ml of solution, agitate, and add 10 drops of conc HF. Allow 10 min for the fluoride precipitate to form and then centrifuge. Discard the supernate, and slurry the precipitate with five drops of saturated H_3BO_3 solution.

---

*Refer to Notes at end of Appendix.

8. Allow the slurry to stand for 5 min. Then add five drops of conc HNO_3 and agitate to effect complete solution. Dilute to 5 ml with H_2O, and precipitate $La(OH)_3$ by bubbling NH_3 through solution for several min. Centrifuge and discard the supernate. Wash with a few ml of H_2O, centrifuge, and discard the wash.

9. Dissolve the precipitate in conc HCl (2 ml), and pass through a one-cm-diameter, one-cm-long Dowex A-1 anion exchange column.[3] Allow the sample to pass through the column, preferably without using air pressure.

10. Wash the column with 2 ml of conc HCl forcing it through by use of a few pounds of air pressure.

11. Repeat step 10.

12. Treat the column with 5 ml of conc HCl-10% HBO_3, forced through by use of a few pounds of air pressure.

13. Wash the column with 5 ml of 12N HNO_3, again using air pressure.

14. Wash the column with 5 ml of conc HCl, using air pressure.

15. Elute the neptunium by allowing 10 ml of 0.1M HCl to pass through the column without using air pressure. (Put this eluant in a CLEAN TUBE.)

16. Evaporate the 0.1M HCl-Np to near dryness. After cooling, take up the residue in three drops of conc HNO_3 and three drops of $HClO_4$. Evaporate the solution to dryness, and cool it.

17. Dissolve the final residue in approximately three drops of 4M HCl. With use of a 100-ml pipette, put the final residue onto a 5-ml platinum disc (preheated to a temperature of about 300°F). Rinse the tube twice with two-drop portions of 4M HCl, and add each rinse to the platinum disc.

18. Allow the plate to evaporate to dryness, flame it and place it on a card holder in preparation for counting.

NOTES

(1) Add the H_2O_2 immediately after the vigorous dissolving action ceases. An excess of H_2O_2 will cause a precipitate to form; consequently, the peroxide should be added dropwise until a light green solution results and all the black material disappears.

(2) Usually use 250 λ of Np^{237} tracer in 4M HCl, giving approximately 800 c/min.

(3) The anion resin used was Ag 1-X8 or 10, 100-200 mesh (Dowex-1), supplied by Bio-Rad Laboratories, 800 Delaware, Berkeley, California. Restore the anion resin as a water slurry, and treat with concentrated HCl before using.

APPENDIX B

Effects of Errors in B:A on Np^{239} Activity Measurements

A successful breeding-gain evaluation requires minimizing errors in the determination of Np^{239} activity. Sources of error affecting the production patterns arise through inadequate counting statistics and an inexact empirical determination of the B:A ratio. The first of these (the effect of counting statistics) is of minor significance and need not be considered. Np^{239} intensity was not a problem, and only under the worst condition did the statistical accuracy of Np^{239} activity determinations approach one percent.

The effect of inaccuracies inherent in the empirical evaluation of the B:A ratio as a function of time is less clear, and the effects of intrinsic uncertainties on the separated Np^{239} component should be considered. The worst possible case involved measurements carried out in a region for which the ratio of capture to fission in U^{238} is small. A typical example of counting data taken for a depleted traverse foil irradiated at the inner edge of the Mark-IV blanket and at centerline elevation is presented in Table B-I. Corrections for foil and environmental backgrounds have been applied to all data listed.

Table B-I

TYPICAL DATA FOR AN IRRADIATED DEPLETED FOIL

	Band A	Band B
Monitor foil	53,288 c/min	2425 c/min
Traverse foil	97,438 c/min	6303 c/min
B/A Ratio	0.681 ± 10%	
Time after irradiation	59 hr	

If an indeterminate random error of ±10% is assumed and statistical considerations (since these are comparatively minor) are neglected, the fission-product component in Band A for the monitor foil is 2425/0.681 ± 10%, or 3561 ± 356. Subtraction of the fission-product component from the Band A activity gives 49,727 ± 356, or ±0.71%. A similar treatment of the traverse-foil data for the Np^{239} activity in Band A gives 88,182 ± 926, or ±1.1%. The ratio of net traverse-foil activity to net monitor activity is then 88,182/49,727, or 1.773 ± 1.3%.

Actually, the effects of errors intrinsic in the value of B/A on the monitor-traverse foil ratio are less than those indicated above, since errors inherent in B:A values are not random (as assumed), but systematic. Hence, division of the traverse-foil activity by the monitor-foil activity tends, to a large extent, to cancel the effects of such errors.

The example above is extreme in that most of the Np^{239} is produced in regions for which the capture-to-fission ratio in U^{238} is large. Accordingly, for increasing distances from the core center, the relative importance of fission products in Band A decreases. For example, in the cup, where the bulk of Np^{239} is produced, practically all the activity in Band A is directly attributable to Np^{239}. Hence, large errors can be tolerated in the values used for B:A.

APPENDIX C

Error Analysis

The reliability of the value established for the breeding ratio may be estimated from the following considerations. Equation (24), which defines the breeding ratio, may be rewritten as

$$B = \frac{a + b}{(c+d) + (e+f) + (g+h)}, \tag{C-1}$$

where

a = Pu^{239} produced,

b = Pu^{241} produced,

c = U^{235} destroyed by fission,

d = U^{235} destroyed by capture,

e = Pu^{239} destroyed by fission,

f = Pu^{239} destroyed by capture,

g = Pu^{241} destroyed by fission,

h = Pu^{241} destroyed by capture,

and

D = (c+d) + (e+f) + (g+h).

Uncertainties inherent in the values of a through h combine statistically to cause uncertainty in the calculated value of B.

The effect of an uncertainty Δa in a on B is given by

$$(\Delta B)_a = \left(\frac{\partial B}{\partial a} \right) \Delta a, \tag{C-2}$$

where the partial derivative $\partial B/\partial a$ is evaluated under the assumption that all other parameters are constant. Similarly, the effect of an uncertainty Δb in b on B is given by

$$(\Delta B)_b = \left(\frac{\partial B}{\partial b} \right) \Delta b. \tag{C-3}$$

Similar expressions apply to the other terms, c through h. The effect of all uncertainties, i.e., $(\Delta B)_a$ through $(\Delta B)_h$, is given by

$$(\Delta B)_{(a-h)} = \sqrt{(\overline{\Delta B})_a^2 + (\overline{\Delta B})_b^2 + \ldots\ldots (\overline{\Delta B})_b^2}. \tag{C-4}$$

Hence,

$$\left(\frac{\partial B}{\partial a}\right) = \frac{1}{D}, \quad \left(\frac{\partial B}{\partial b}\right) = \frac{1}{D}, \quad \left(\frac{\partial B}{\partial c}\right) = \frac{-(a+b)}{D^2}, \quad \left(\frac{\partial B}{\partial d}\right) = \frac{-(a+b)}{D^2},$$

$$\left(\frac{\partial B}{\partial e}\right) = \frac{-(a+b)}{D^2}, \quad \left(\frac{\partial B}{\partial f}\right) = \frac{-(a+b)}{D^2}, \quad \left(\frac{\partial B}{\partial g}\right) = \frac{-(a+b)}{D^2}, \quad \left(\frac{\partial B}{\partial h}\right) = \frac{-(a+b)}{D^2},$$

and

$$(\Delta B)_a = \frac{\Delta a}{D}, \quad (\Delta B)_b = \frac{\Delta b}{D}, \quad (\Delta B)_c = \frac{-\Delta c\,(a+b)}{D^2}, \quad (\Delta B)_d = \frac{-\Delta d\,(a+b)}{D^2},$$

$$(\Delta B)_e = \frac{-\Delta e\,(a+b)}{D^2}, \quad (\Delta B)_f = \frac{-\Delta f\,(a+b)}{D^2}, \quad (\Delta B)_g = \frac{-\Delta g\,(a+b)}{D^2},$$

$$(\Delta B)_h = \frac{-\Delta h\,(a+b)}{D^2}.$$

In evaluating the error effects $(\Delta B)_a$ through $(\Delta B)_h$ actual values must be assigned the uncertainties Δa through Δh. These uncertainties are summarized in Table C-I, in both percentage units and absolute values.

Table C-I

UNCERTAINTY ASSIGNMENTS

Variable	Uncertainty	Value from Table XVIII	Uncertainty Absolute Units
a	5%	1.492	0.0746
b	20	0.0055	0.0011
c	5	0.1420	0.0071
d	10	0.0360	0.0036
e	5	0.9146	0.0457
f	10	0.0841	0.0084
g	20	0.0054	0.0011
h	20	0.0005	0.0001

Tables C-I and XVIII indicate that the respective values of $(\Delta B)_a$ through $(\Delta B)_h$ are 0.0631, 0.0093, 0.00764, 0.00390, 0.004899, 0.00899, 0.001198, and 0.00015. Substitution of these values into equation (C-4) results in a value of ± 0.08. On a percentage basis, the resultant uncertainty is $\pm 0.08/1.27$, or $\pm 6.3\%$.

REFERENCES

1. Zinn, W. H., et al , Feasibility Report, Fast Neutron Pile for Test of Conversion, ANL-4356 (October 14, 1949).

2. Lichtenberger, H V., Operating Experience and Experimental Results Obtained from a NaK-Cooled Fast Reactor, Proc. of the Int. Conf. on the Peaceful Uses of Atomic Energy, United Nations, New York, 3, 345 (1955).

3. Lichtenberger, H. V., et al., Experimental Breeder Project Report for the Period December 1948 through February 28, 1949, ANL-4274 (April 12, 1949).

4. Lichtenberger, H. V., et al., Experimental Breeder Project Report for the Period March 1, 1949 through January 31, 1959, ANL-4420 (March 13, 1950).

5. Lichtenberger, H. V . et al., Experimental Breeder Project Report for the Period February 1, 1950 through March 31, 1951, ANL-4554 (April 1, 1951).

6. Lichtenberger, H. V., et al , Experimental Breeder Project Report for the Period April 1, 1951 through January 31, 1953, ANL-5023 (February 20, 1953)

7. Brittan, R. O., Analysis of the EBR-I Core Melt-down, Proceedings of the Second United Nations Int. Conf. on the Peaceful Uses of Atomic Energy, Geneva, Switzerland, 12, 267 (1958).

8. Kittel, J. H., Novick, M., and Buchanan, R F., The EBR-I Meltdown, Physical and Metallurgical Changes in the Core, Nuclear Science and Engineering, 4(2), 180 (1958).

9. Rice, R. E., et al., EBR-I, Mark III Design, ANL-5836 (March 1958).

10. Thalgott, F. W., et al., Stability Studies on EBR-I, Proceedings of the Second United Nations Int. Conf. on the Peaceful Uses of Atomic Energy, Geneva, Switzerland, 12, 242 (1958).

11. Smith, R. R., et al., Instability Studies with EBR-I, Mark III, ANL-6266 (Dec 1960).

12. Smith, R. R., et al., A Mechanism Explaining the Instability of EBR-I, Mark II, ANL-6354 (Sept 1961).

13. Levenson, Milton, Determination of the Conversion Ratio of the Experimental Breeder Reactor by Radiochemical Methods, ANL-5095 (Dec 19 3).

14. Curtis, C. D., et al., A Physical Determination of the Conversion Ratio of the Experimental Breeder Reactor, ANL-5222 (Aug 1954).

15. Kato, W. Y., et al., Measurements of the Conversion Ratio for a Fast Breeder Reactor, First Nuclear Engineering and Science Congress, Cleveland, Ohio, Vol. II, Reactor Operational Problems, Pergamon Press, New York (1957)

16. Haroldsen, R. O., et al., Safety Analysis Report, EBR-I, Mark IV, ANL-6411 (Feb 1963).

17. Burt, W., Argonne National Laboratory, private communication.

18. Spinrad, B. I., Proceedings of the Conference on the Physics of Breeding, p. 23, ANL-6122.

19. Graham, R. L., and Bell, R. E., Disintegration of Np^{239}, Phys. Rev., 222 (1951).

20. Heath, R. L., Scintillation Spectrometry, Gamma Ray Spectrum Catalogue, IDO-16408 (July 1957).

21. Vegors, S. H., et al., Calculated Efficiencies of Cylindrical Radiation Detectors, IDO-16370 (Sept 1, 1958).

22. Axtmann, R. C , and Stutheit, J. S., Scintillation Counting of Natural Uranium Foils, Nucleonics, 12(7), 52 (July 1954).

23. Brunson, G. S., Design and Hazards Report for the Argonne Fast Source Reactor (AFSR), ANL-6024 (June 1959).

24. Crouthamel, C. E., Applied Gamma Ray Spectrometry, Pergamon Press, New York (1960).

25. McGinnis, F. D., private communication.

26. Kafalas, P., et al., Determination of the Ratio of Capture to Fission Cross Sections in EBR-I, Nuclear Science and Engineering, 2(5), 657 (1957).

27. Rein, J. E., Phillips Petroleum Company, private communication.

28. Armani, Roland, Argonne National Laboratory, private communication.

29. Cowan, G., Los Alamos Scientific Laboratory, private communication.

30. Yiftah, S., et al., Fast Reactor Cross Sections, Pergamon Press, New York (1960).

31. Davey, W. G., Argonne National Laboratory, private communication.

32. Okrent, D., and Thalgott, F. W., Proceedings of the Conference on Plutonium as a Power Reactor Fuel, HW-75007 (Dec 1962).